



RESEARCH ARTICLE

10.1002/2016GC006554

Key Points:

- Seismic surveys and geochemical analyses were combined to study a cluster of hydrate-bearing pockmarks
- The pockmark dynamics is governed by fluid flow
- Sulfate-profile simulation allowed estimating the formation age of four selected hydrate layers

Supporting Information:

- Supporting Information S1

Correspondence to:

L. Ruffine,
livio.ruffine@ifremer.fr

Citation:

de Prunelé, A., et al. (2017), Focused hydrocarbon-migration in shallow sediments of a pockmark cluster in the Niger Delta (Off Nigeria), *Geochem. Geophys. Geosyst.*, 18, 93–112, doi:10.1002/2016GC006554.






Received 1 AUG 2016

Accepted 9 DEC 2016

Accepted article online 29 DEC 2016

Published online 19 JAN 2017

Focused hydrocarbon-migration in shallow sediments of a pockmark cluster in the Niger Delta (Off Nigeria)

Alexis de Prunelé^{1,2}, Livio Ruffine¹ , Vincent Riboulot¹, Carl A. Peters³, Claire Croguennec¹, Vivien Guyader¹ , Thomas Pape³ , Claire Bollinger², Germain Bayon¹, Jean-Claude Caprais⁴, Yoan Germain¹, Jean-Pierre Donval¹ , Tania Marsset¹, Gerhard Bohrmann³, Louis Géli¹, Abdulkarim Rabiou⁵, Marc Lescanne⁶, Eric Cauquil⁶, and Nabil Sultan¹ 

¹IFREMER, Département Ressources physiques et Ecosystèmes de fond de Mer (REM), Unité des Géosciences Marines, Plouzané, France, ²Institut Européen de la Mer (IUEM), Ecole doctorale des Sciences de la mer, Plouzané, France, ³MARUM Center for Marine Environmental Sciences, Leobener Str., Bremen, Germany, ⁴IFREMER, Département Ressources physiques et Ecosystèmes de fond de Mer (REM), Unité des Ecosystèmes Profonds, Plouzané, France, ⁵Nigeria Institute for Oceanography and Marine Research, Nigeria, ⁶TOTAL Exploration Production, France

Abstract The Niger Delta is one of the largest hydrocarbon basin offshore Africa and it is well known for the presence of active pockmarks on the seabed. During the Guineco-MeBo cruise in 2011, long cores were taken from a pockmark cluster in order to investigate the state of its current activity. Gas hydrates, oil, and pore-water were sampled for geochemical studies. The resulting dataset combined with seismic data reveal that shallow hydrocarbon migration in the upper sedimentary section was focused exclusively within the pockmarks. There is a clear tendency for gas migration within the hydrate-bearing pockmarks, and oil migration within the carbonate-rich one. This trend is interpreted as a consequence of hydrate dissolution followed by carbonate precipitation in the course of the evolution of these pockmarks. We also demonstrate that Anaerobic Oxidation of Methane (AOM) is the main process responsible for the depletion of pore-water sulfate, with depths of the Sulfate-Methane Transition Zone (SMTZ) ranging between 1.8 and 33.4 m. In addition, a numerical transport-reaction model was used to estimate the age of hydrate-layer formation from the present-day sulfate profiles. The results show that the sampled hydrate-layers were formed between 21 and 3750 years before present. Overall, this work shows the importance of fluid flow on the dynamics of pockmarks, and the investigated cluster offers new opportunities for future cross-site comparison studies. Our results imply that sudden discharges of gas can create hydrate layers within the upper sedimentary column which can affect the seafloor morphology over few decades.

1. Introduction

Pockmarks are defined as surface depressions on the seafloor typically characterized by circular or elongated crater shapes, e.g., [King and MacLean, 1970]. Their sizes vary from less than one to several hundreds of meters width and from less than one to tens of meters depth [Hovland and Judd, 1988; Hovland et al., 2002]. On continental margins, pockmarks are often associated with shallow fluid migration. Numerous investigations have been carried out in order to better understand the effects of fluid flow on the dynamics of pockmarks, i.e., their formation and evolution, both spatially and temporally [Andresen et al., 2008; Berndt, 2005; Betzler et al., 2011; Cathles et al., 2009; Chen et al., 2010; Gay, 2002; Gay et al., 2006; Ho et al., 2012; Hovland and Judd, 1988; Josenhans et al., 1978; Judd and Hovland, 2007; Luo et al., 2015; Moss et al., 2012; Riboulot et al., 2014; Rise et al., 1999; Sultan et al., 2010, 2014]. Thus, several conceptual models, based on fluid migration, have been proposed to explain their formation process. The arrival of upward-migrating fluids throughout the sedimentary column to the seafloor can cause the fluidization of the surficial sediment, triggering its resuspension and dispersion into the water column [Hovland and Judd, 1988; Josenhans et al., 1978]. The redeposition of the previously suspended sediments might be prevented by the occurrence of a continuous gas plume. Thus, sediment focusing and deposition take place mainly at the periphery of the plume, leading to the formation of a depression by differential sedimentation [Chand et al., 2009; Gay, 2002; León et al., 2010; Moss et al., 2012; Ostanin et al., 2013].

In geological settings characterized by hydrate-bearing sediments, Sultan et al. [2010, 2014] have claimed that rapid formation combined with slow dissolution of hydrates are key processes that cause pockmark

formation and evolution. Indeed, hydrate-bearing pockmarks often reveal a complex seafloor morphology that may result from the formation and/or decomposition of gas hydrates in the underlying sedimentary layers [Davy *et al.*, 2010; Macelloni *et al.*, 2012; Nakajima *et al.*, 2014; Riboulot *et al.*, 2016; Simonetti *et al.*, 2013; Sultan *et al.*, 2010, 2014]. Riboulot *et al.* [2016] showed that the mechanism which drives pockmark development off Nigeria is the formation of conical fractures induced by the formation of gas hydrates. Besides, Nakajima *et al.* [2014] proposed another pockmark-formation mechanism and suggested that hydrate dissociation triggered by sea-level fall during the Last Glacial Maximum (LGM) may induce the expulsion of methane and sand into the water column. This expulsion of materials can change mounds into pockmarks due to a progressive collapse of the former. Nickel *et al.* [2012] also consider that pockmark formation in the SW-Barents Sea has started during the LGM. The thaw and regression of the ice sheet induced a decrease of the hydrostatic pressure, resulting in hydrate decomposition within the sedimentary column and methane release into the water column, and ultimately leading to the formation of pockmarks at the seafloor. Recently, Pape and coworkers [Pape *et al.*, 2011] have shown that fluid expulsion in the water column may also cause detachment and rafting of outcropping hydrate blocks, creating small holes or craters which could be the inception of pockmark formation. The methane constituting the hydrates is either of thermogenic sources and come from deep-hydrocarbon reservoirs or of microbial sources, and in this case, it is generated at shallow depths [Whiticar, 1994]. Methane is transported within the sediment as dissolved species in the interstitial fluid, or as free gas leading to methane ebullition at the seafloor [Noethen and Kasten, 2011].

The present paper focuses on the influence of fluid flow, more particularly hydrocarbon-rich fluids, on the dynamics of a pockmark cluster on the Nigerian continental slope. It combines measurements of pore-water dissolved elements together with seismic data, and aims to constrain the hydrocarbon migration pattern in this area. Sultan *et al.* [2010] showed different morphologies of gas hydrate pockmarks. They suggest that these morphologies correspond to five different phases of pockmark evolution during hydrate formation and dissolution. This work complements the study of Sultan and coworkers, by dealing with the influence of fluid flow within these geological features.

2. Description of the Study Area

2.1. Regional Description of the Niger Delta

The study area is located in the Niger Delta deep-province on the west coast of Central Africa, off Nigeria. The submarine Niger Delta is composed of successive sedimentary deposits which form the most extensive deltaic system in Africa [Cohen and McClay, 1996]. These deposits lead to the southward progradation of the margin into the Gulf of Guinea [Burke, 1972]. The resulting sedimentary prism has gradually expanded and now covers a seafloor area of about 140,000 km² with a maximum thickness of 12 km [Damuth, 1994]. This delta is also characterized by gravity-driven tectonism due to rapid sediment loading [Bilotti and Shaw, 2005; Corredor *et al.*, 2005; Damuth, 1994; Riboulot *et al.*, 2012]. The investigated area is located at water depth ranging between 1100 and 1250 m, and covers an area of about 20 km². Its subsurface is characterized by the presence of numerous buried channels, which were likely generated from gas accumulation followed by discharge within the clay-rich sediment when the gas pressure exceeds the pressure of the overlaid sedimentary and water columns [Sultan *et al.*, 2014]. It has been the subject of intensive investigations by both industry and academia with four main French scientific cruises: *NERIS* (2003 and 2004) and *ERIG-3D* (2008) and more recently *Guineco-MeBo* (2011). The latter has been undertaken onboard the French *R/V Pourquoi pas?* in the frame of a scientific collaboration between IFREMER and MARUM, and was devoted to the investigation of a pockmark-prone area using a multidisciplinary approach.

2.2. Seabed Morphology of the Pockmark Cluster

The bathymetric map in Figure 1b revealed a field of pockmarks with variable diameters. The cluster of interest here is represented in Figure 1a and in the black rectangle of Figure 1b. The northernmost depression is called Pockmark-B. It is characterized by an ellipsoidal shape, with an N-S-oriented principal axis of ~735 m and E-W-oriented second axis of ~500 m. It also corresponds to the deepest depression with a crater of around 60 m depth. Gas hydrates have not been recovered from this pockmark although a core of >20 m-length has been retrieved. Instead, it was characterized by the presence of widespread carbonate concretions and oil pockets. The three remaining pockmarks called pockmark-C1, pockmark-C2, and

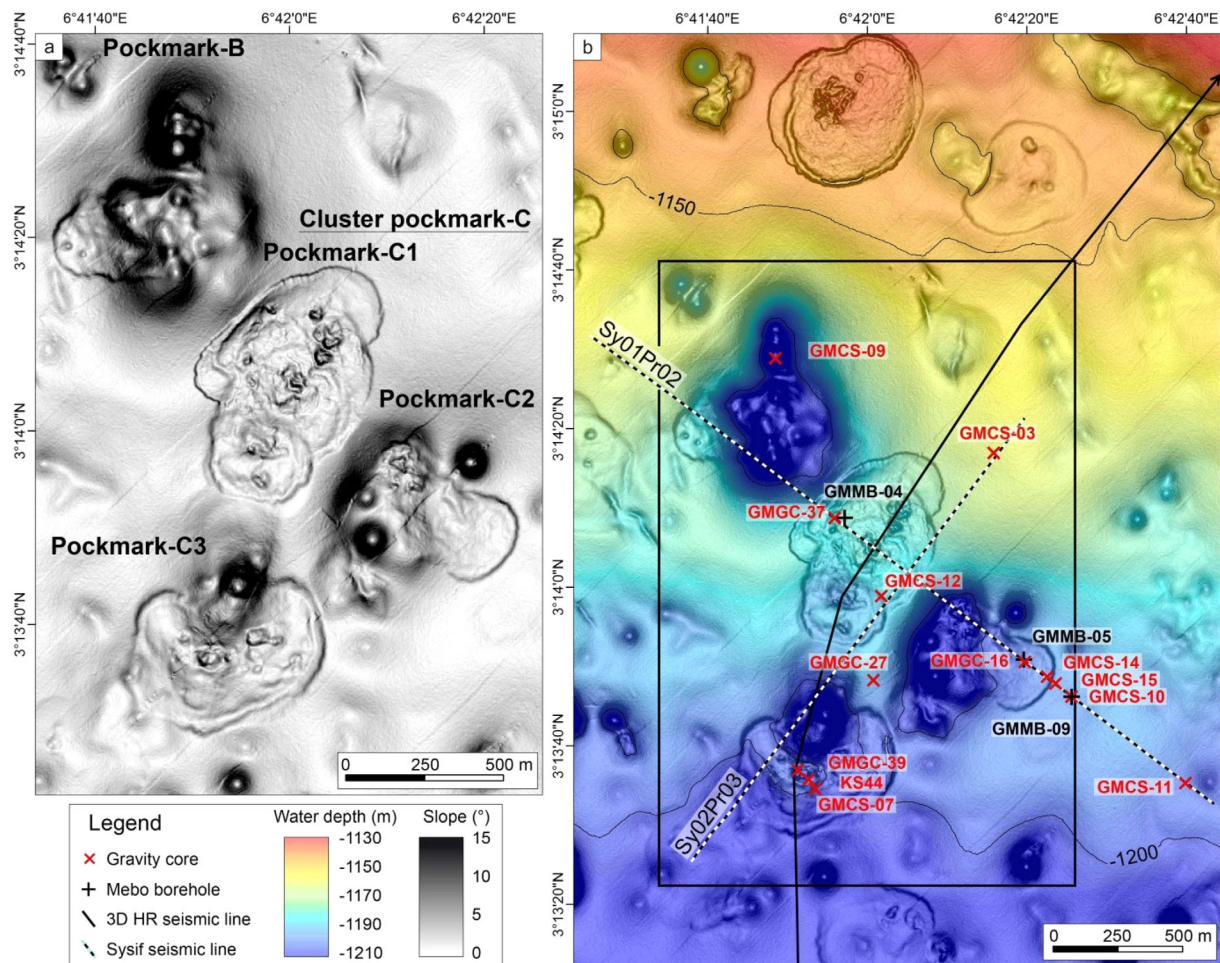


Figure 1. Bathymetric map of the investigated area: (a) Dip map showing geomorphology of the cluster Pockmark-C and Pockmark-B; (b) Localization of the collected cores, the VHR seismic profiles from the SYSIF and the 3D HR seismic line.

pockmark-C3 have a diameter ranging between 500 and 800 m (Figure 1). Gas hydrates have been both inferred from seismic data [Sultan *et al.*, 2010] and also recovered from cores for all three pockmarks [Wei *et al.*, 2015]. Thus, they form a hydrate-bearing cluster hereby called Pockmark-C. The pockmark-C1 is an ellipsoidal depression with a NE-SW-oriented principal axis of ~ 800 m and NW-SE-oriented second axis of ~ 500 m. Pockmark-C2 is located southeast from pockmark-C1. It has also an ellipsoidal shape with a NNE-SSW-oriented principal axis of ~ 540 m and NNW-SSE-oriented second axis of ~ 615 m. Pockmark-C3 is located at the southern part of the cluster. It shows a nearly circular shape and has a diameter of about ~ 600 m. The three pockmarks show irregular seabed morphology with rough and distorted circle-like ripples. Their peripheral zone consists of a pronounced ring characterized by a high dip, with values reaching 10° . All four studied pockmarks are characterized by moats and bulges on their surface in variable number and distribution.

3. Sampling and Analytical Methods

3.1. Coring Strategy and Pore Water Extraction

Cores were recovered using either the Calypso length-variable gravity piston corer from IFREMER (core code GMCS-XX), a 6m-length gravity corer equipped with a plastic bag (core code GMGC-XX) or the seafloor drill rig MeBo from MARUM [Wei *et al.*, 2015] (core code GMMB-XX). The gravity corer was used at location where very shallow gas hydrates were suspected as it enables very quick recovery and effective hydrate-sampling from sediments disturbed as less as possible. The seafloor drill rig MeBo was used to

recover cores of tens of meters length, while Calypso core was a compromise between the two other coring technics. The quality and length of the recoveries were strongly related to the presence and the amount of hydrates within the sediments. Overall, the recovery was of good quality, with local muddy sediment interval due to hydrate dissociation [Wei *et al.*, 2015]. The locations of the collected cores are shown in Figure 1b. In order to study the influence of fluid flow on the pockmark dynamics, most of the cores have been collected along two predetermined seismic profiles SY02-HR-PR03 and SY01-HR-PR02 (this will be detailed below), or as close as possible to them; except for core GMCS-09 which has been taken in pockmark-B. Cores GMCS-11, GMCS-10 and GMCS-15 were collected outside the depressions, at around 585 m, 95 m, and 35 m away from the rim of pockmark-C2, respectively. Cores GMCS-14, GMCS-16, GMMB-05 were taken within pockmark-C2, and a distance of only 65 m separates GMCS-14 and GMCS-15. Both GMCS-12 and GMGC-37 were retrieved from pockmark-C1 while cores GMCS-07 and GMGC-39 were recovered on pockmark-C3. Core GMGC-27 was located at the middle of the cluster (Figure 1b).

Immediately after recovery, Calypso cores were cut into sections of 1 m length and transferred into the cold laboratory at 4°C for pore-water extraction. This was done using the Rhizon® soil moisture sampler. The sampler consists of a hydrophilic porous polymer tube of 2.5 mm diameter and 50 mm length [Dickens *et al.*, 2007; Seeberg-Elverfeldt *et al.*, 2005] which is introduced into the sediment and connected to an evacuated syringe of 10 mL. The plastic bag of the gravity corer was taken out and opened for direct Rhizon® sampling. The decision to sample pore waters from the gravity cores was taken after a visual inspection to check the good preservation of the sediment. In the case of the MeBo cores, each liner of 2.52 m length was kept uncut for pore water extraction. The collected pore water was split into two subsamples: One subsample was poisoned with sodium azide to prevent any subsequent microbial activity and used for light hydrocarbon (C₁–C₅) analyses [Alberto *et al.*, 2000]. The second subsample was stored within a pre-evacuated vial for measurement of dissolved elements. All samples were kept at –5°C for onshore analyses at IFREMER.

3.2. Methods and Analyses

3.2.1. Seismic Survey

A set of 2D Very High Resolution (VHR) near-bottom echo-sounder data acquired using an Autonomous Underwater Vehicles (AUV) operated by C&C Technologies Survey was used to provide a detailed map of the near seafloor and the bathymetry. The two VHR seismic profiles SY01-HR-PR02 and SY02-HR-PR03 were acquired during the ERIG-3D cruise [Ker *et al.*, 2010; Sultan *et al.*, 2010] using a deep-towed seismic device called SYSIF (Système Sismique Fond) equipped with two Janus–Helmholtz acoustic transducers (580–2200 Hz and 220–1050 Hz) from IFREMER [Ker *et al.*, 2010; Marsset *et al.*, 2010]. They enable a precise description of the shallow internal structure of the pockmarks (Figures 2b and 3b). The acquisition was performed with a vertical resolution of 30 cm, a horizontal resolution of 6 m, and a maximum total penetration of 100 ms (two-way travel time, TWT). To complete our seismic dataset, we also used a line extracted from a 3D High Resolution (3D HR) seismic block belonging to Total oil company [George and Cauquil, 2007], and crossing lengthwise pockmark-C1 and pockmark-C3 (Figure 4).

3.2.2. Pore-Water Analyses

Pore-water samples were analyzed either during the cruise or at the IFREMER laboratory. Thus, directly after extraction, 1 mL of pore-water was used to measure total alkalinity (Alk) with a titrimeter 848 Titrino Plus (Metrohm) using a solution of 0.1N HCl. Sulfate (SO₄²⁻) and chloride (Cl⁻) were analyzed on board using an ionic chromatograph (Metrohm 861, Advanced Compact IC) calibrated with the standard seawater from the International Association for Physical Sciences of Oceans (IAPSO). The concentration values were determined with an estimated accuracy better than ±3%.

Concentrations of light dissolved-hydrocarbons (C₁–C₅) were measured using a gas chromatograph (Perichrom® PR 2100) equipped with a headspace injector (Dani HSS 86.50) and a Flame Ionization Detector (FID). A temperature program starting from 60°C and ending at 180°C was applied. The instrument was calibrated using a certified gas-mixture (Air Liquide) containing 1.45, 1.022, 1.039, 1.033, and 1.062 in mol % for methane, ethane, propane, *n*-butane, and pentane, respectively. The claimed accuracy is of 2% in molar fraction for all components. $\Delta^{13}\text{C-CH}_4$ measurements were performed with a G2201-*i* Cavity Ring-Down Spectroscopy Analyzer (CRDS from Picarro®, California). The instrument was calibrated against four gas standards (Isometric Instruments) having a $\delta^{13}\text{C-CH}_4$ of –23.9, –38.3, –54.5, and –66.5 per mil (‰),

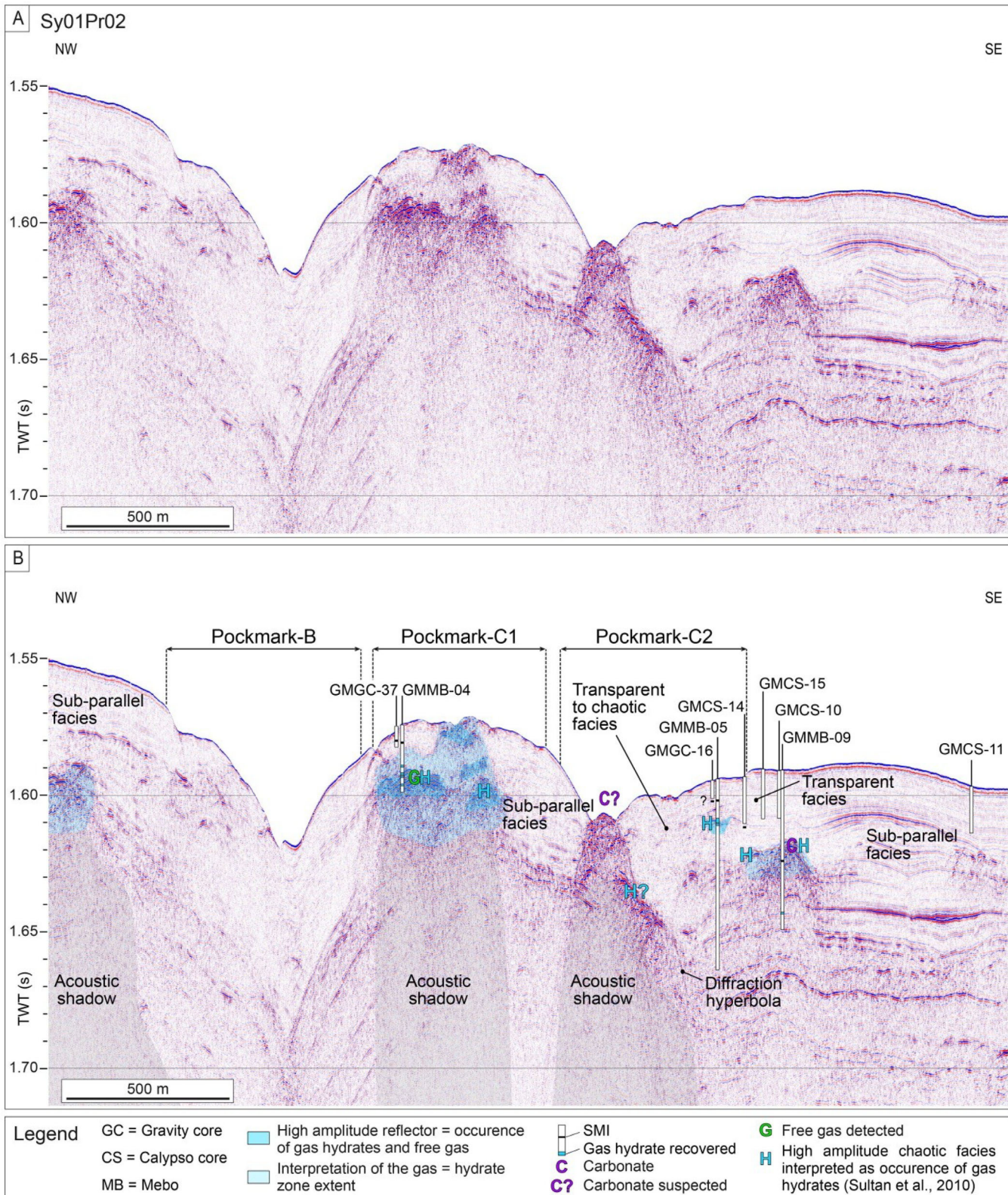


Figure 2. (a) Uninterpreted 2D very high resolution seismic profiles (acquired with the SYSIF, SY01-HR-PR02), showing fine details of the shallow sedimentary column of pockmark-B, pockmark-C1 and pockmark-C2 (modified from Sultan et al., 2010). (b) The interpretation of the seismic profile, together with core observations and geochemical analyses, showed the occurrence of gas hydrates inside the pockmarks C1 and C2. This corresponds to high amplitude chaotic seismic facies. The SMTZ, identified from pore-water analyses, is located above and close to the upper gas hydrate layers.

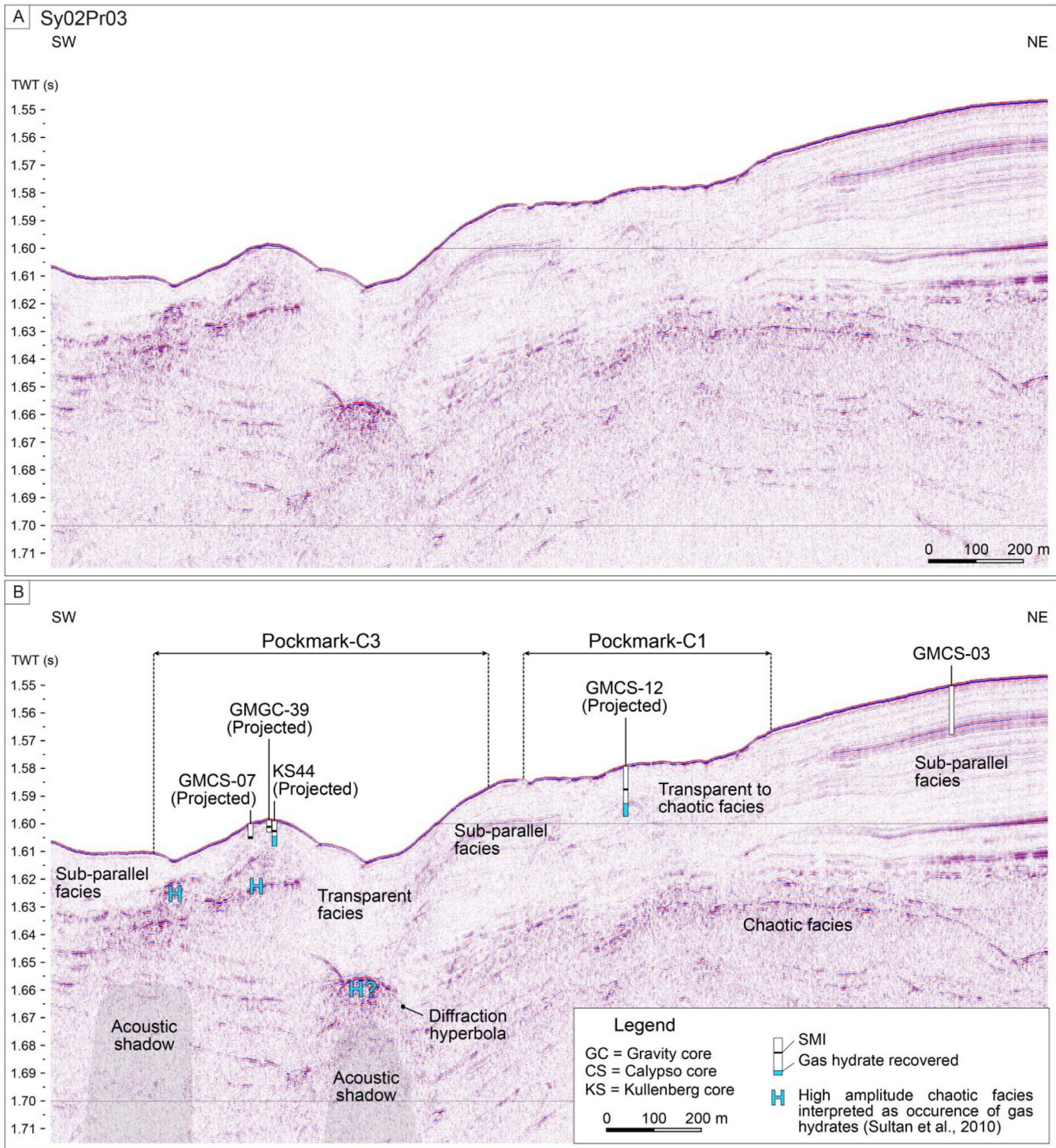


Figure 3. (a) Uninterpreted 2D very high resolution seismic profiles (acquired with the SYSIF, SY02-HR-PR03, showing fine details of the shallow sedimentary column of pockmark-C1 and pockmark-C3 (modified from Sultan et al., 2010). (b) The interpretation of the seismic profile, together with core observations and geochemical analyses, showed the occurrence of gas hydrates inside the pockmarks C1 and C3. This corresponds to high amplitude chaotic seismic facies. The SMTZ, identified from pore-water analyses, is located above and close to the upper gas hydrate layers.

respectively. Only samples with a significant amount of dissolved methane ($>4 \mu\text{mol L}^{-1}$) were eligible for the measurement of stable carbon isotopic ratios. Thus, $\delta^{13}\text{C-CH}_4$ was not measured for the cores collected outside the pockmarks. It was also not measured for the MeBo cores.

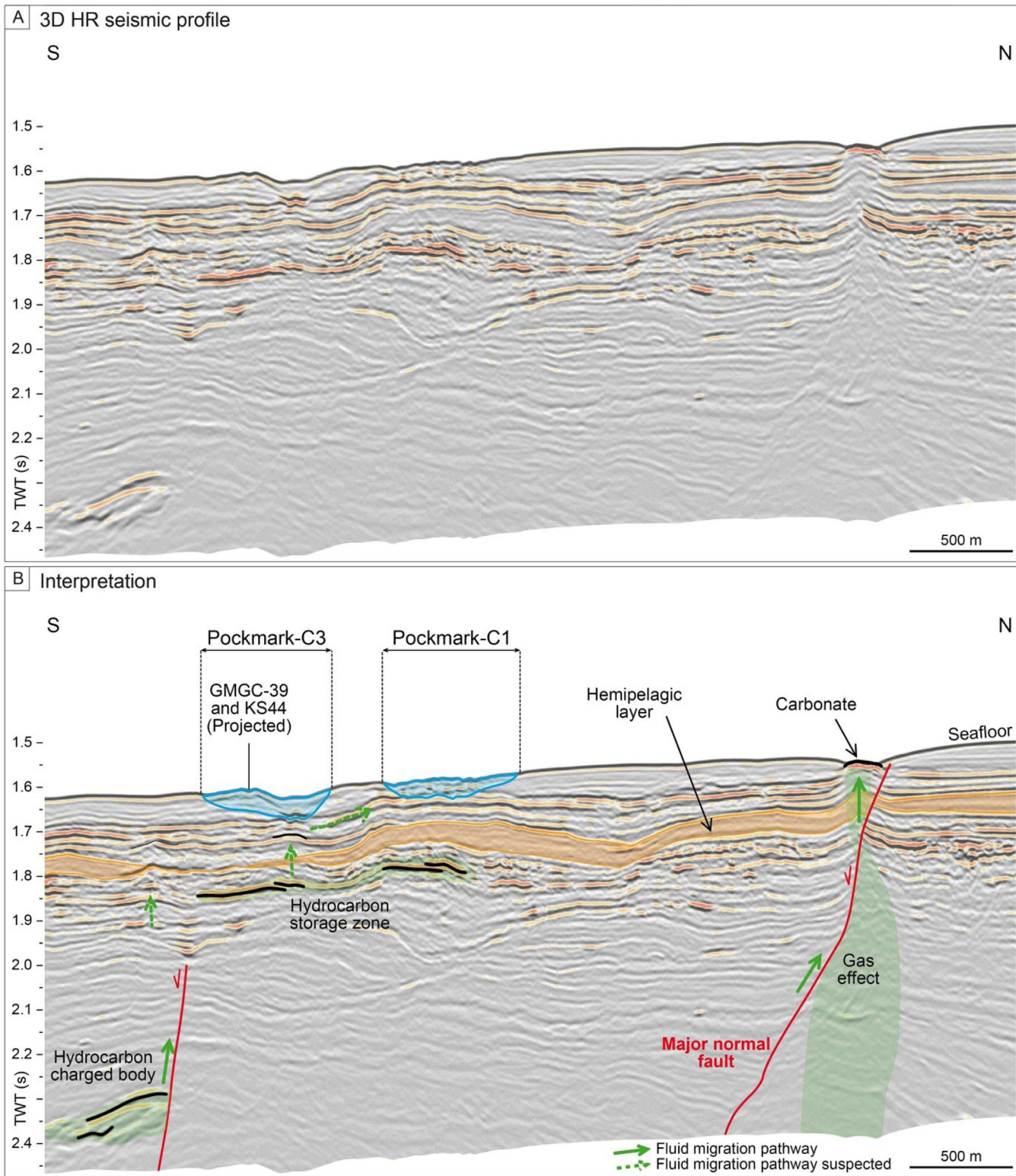


Figure 4. (a) Random line extracted from a 3D HR seismic block (courtesy of Total) showing a broad view of the plumbing system. (b) Interpretation of the seismic line: it reveals the presence of both deep and shallow hydrocarbon charged bodies. Faults (red lines) constitute the preferential gas migration pathway (green arrows) from depth and supply gas to the shallowest gas storage zone located under the hydrate-bearing pockmarks C1 and C3.

3.2.3. Gas-Hydrate Analyses

Pieces of hydrate were placed into a 10 mL sealed glass vial. The latter was evacuated to avoid air contamination, and then the hydrate was allowed to decompose at ambient temperature. The hydrate-bound gases were collected into a 12 mL pre-evacuated glass vial and sent to Isolab (Netherlands) for both isotopic and molecular composition analyses. Molecular composition, $\delta^{13}\text{C}$ and δD were measured using a GCC-IRMS, with an analytical precision of $\pm 2\%$, $\pm 0.1\text{--}0.3\text{‰}$ and $\pm 1\text{--}3\text{‰}$, respectively.

3.2.4. Oil Analyses

Oil analyses were performed at Isolab (Netherlands). The oil sample was split in subsamples. One subsample was topped in order to perform SARA (Saturate, Aromatic, Resin, and Asphaltene) analysis. Thus, the sample was put into a vacuum oven for 72 h at 60°C and 50–100 mbar. The separation of the topped oil in Topped Saturate (TS), Topped Aromatic (TA), Topped Resin (TR) and Topped Asphaltene (TAs) fractions was done by Medium Pressure Liquid Chromatography (MPLC). Packed columns with different sizes of silica were used as stationary phase and n-hexane as mobile phase. During the whole process, the total weight loss was of 22.5%, and corresponds to the lighter fraction subject to evaporation. Gas chromatography analysis was performed on the untopped subsample, while 2D (GCxGC) gas chromatography analysis was done on both the untopped subsample and the TS fraction.

3.2.5. Numerical Modeling of the AOM

A numerical transport-reaction model was developed in gPROMS software (Process System Enterprise, PSE Ltd) to describe the AOM reaction, the transport processes of the studied solutes and the evolution of the SMTZ over time. The model is based on the diagenetic equations [Berner, 1980; Boudreau, 1997]. It takes into account the molecular diffusion of methane and sulfate, advection of fluids, as well as the AOM reaction rate. It is expressed as follows:

$$\Phi \frac{\partial [C_i]}{\partial t} = \frac{\partial}{\partial x} \left[\Phi \frac{D_i}{\vartheta^2} \frac{\partial [C_i]}{\partial x} \right] + \Phi v \frac{\partial [C_i]}{\partial x} - \Phi R_{AOM} \quad (1)$$

Where t is time (yr), Φ is the sediment porosity, x is the depth within the sedimentary column (m), ϑ is the sediment tortuosity, C_i and D_i are the concentration (mM) and diffusion coefficient ($\text{m}^2 \text{ yr}$) of the dissolved species i , respectively, v is the upward fluid velocity, and R_{AOM} is the reaction rate. The sediment porosity was a function of depth and obtained by fitting measured profiles with the following equation [Boudreau, 1997]:

$$\Phi(x) = \Phi_f + (\Phi_0 - \Phi_f)e^{-px} \quad (2)$$

Where Φ_0 and Φ_f are porosity at depths zero and infinite, respectively; and p is the fitted attenuation coefficient indicating the decrease of porosity with depth. These values were measured from the reference MeBo core GMMB-03. Values of 0.80 and 0.65 were found for Φ_0 and Φ_f , respectively.

The sediment tortuosity is obtained using Boudreau empirical formulation:

$$\theta^2 = 1 - \ln(\Phi^2) \quad (3)$$

The AOM rate was expressed by the following kinetic equation:

$$R_{AOM} = k_{AOM} [\text{SO}_4][\text{CH}_4] \quad (4)$$

Table 1. Parameters Used in the Numerical Model

| Parameter | Symbol | Unit | Value | | | |
|--|---|----------------------------------|-----------------------|-----------------------|-----------------------|-------------------------|
| | | | GMCS-12 From C1 | GMCS-14 From C2 | GMCS-07 From C3 | GMMB-09 From Outside |
| Model domain | L | M | 7.7 | 20.5 | 4.5 | 38.5 |
| Molecular diffusion coefficient, SO_4 | D_{SO_4} | $\text{m}^2 \text{ sec}^{-1}$ | $5.51 \text{ E} - 10$ | $5.51 \text{ E} - 10$ | $5.51 \text{ E} - 10$ | $5.51 \text{ E} - 10$ |
| Molecular diffusion coefficient, CH_4 | D_{CH_4} | $\text{m}^2 \text{ sec}^{-1}$ | $8.62 \text{ E} - 10$ | $8.62 \text{ E} - 10$ | $8.62 \text{ E} - 10$ | $8.62 \text{ E} - 10$ |
| SO_4 concentration at the sediment surface | $[\text{SO}_4]$ | mM | 28.7 | 28.7 | 28.7 | 28.7 |
| CH_4 concentration at the sediment surface | $[\text{CH}_4]$ | mM | 0 | 0 | 0 | 0 |
| CH_4 concentration at lower boundary domain | $[\text{CH}_4]$ | mM | 64 | 64 | 64 | 64 |
| SO_4 flux at lower boundary domain | $\frac{\partial [\text{SO}_4]}{\partial x}_L$ | mM m^{-1} | 0 | 0 | 0 | 0 |
| Upward fluid velocity | v | cm yr^{-1} | 0 | 0 | 0 | 0 |
| AOM constant rate | k_{AOM} | $\text{mM}^{-1} \text{ yr}^{-1}$ | $32 \text{ E} - 02$ | $32 \text{ E} - 02$ | $32 \text{ E} - 02$ | $32 \text{ E} - 02$ |

Table 1 summarizes the parameter values used for the modeling. The methane sourcing the AOM comes from the hydrates. Thus, the lower boundary domain was taken as the top of the GHOZ, and was determined either visually after the core splitting, by infrared thermal imaging [Wei *et al.*, 2015] or from chloride anomalies due to pore water freshening. The methane concentration at the boundary domain was calculated from the online Duan's Research Group thermodynamics model [Sun and Duan, 2007].

4. Seismic Data Interpretation and Geochemical Results

4.1. Shallow Internal Architecture of the Pockmark Cluster

The VHR seismic sections crossing the studied pockmarks show the detail architecture of the shallow sedimentary layers (Figures 2 and 3). The seismic facies are continuous and sub-parallel outside the seabed deformations. The sedimentary layers outside the pockmarks are characterized by local interruptions at the peripheral of these structures. This, together with the occurrence of seismic reflections under the pockmarks, suggests the presence of deformed sediment or fluid chimneys. The area underlying the cluster Pockmark-C is characterized by the presence of a high-amplitude chaotic seismic facies combined with a transparent facies and the absence of an associated vertical chimney (Figures 2 and 3). These seismic facies have approximately the same horizontal extent as the seabed pockmarks. Figures 2 and 3 also show the presence of free gas within the GHOZ as demonstrated from previous studies of the pockmark cluster by Sultan and coworkers [Sultan *et al.*, 2007, 2014]. Such a coexistence is not commonly encountered at hydrate-bearing setting and has been observed in the Yaquina Forearc Basin off Peru, at Hydrate Ridge off Oregon and the Woolsey Mound in the Gulf of Mexico [Macelloni *et al.*, 2012; Milkov *et al.*, 2004; Netzeband *et al.*, 2005; Simonetti *et al.*, 2013]. We believe that the coexistence of free gas together with gas hydrates for our pockmark cluster results from a sudden gas release followed by a rapid hydrate growth [Sultan *et al.*, 2014], and it is not due to the occurrence of an ascending gas-charged brine as proposed by Milkov *et al.* [2004].

4.2. Deep Plumbing of the Cluster

The 3D HR seismic line in Figure 4 provides a broad view of the plumbing of the area, where two high amplitude reflector packages are interpreted as being two hydrocarbon-charged bodies at around 150–170 and 500–580 mbsf. The deepest one is connected to a normal fault which does not reach the seafloor unlike the normal fault located further north (Figure 4), but it is rather connected to a horizontal channel at ~250 mbsf. The shallowest hydrocarbon-charged body is covered by a sedimentary layer which is interpreted as a regional hemipelagic layer, acting as an impermeable caprock for storage. However, its thickness is thinner just above the hydrocarbon-charged body, and this would enhance the migration of fluid from depth. The resolution of our seismic profiles does not allow the identification of small-scale pathways for migration, i.e., faults, fractures or conduits, directly connected to the pockmarks. However, we believe that such pathways are likely present, possibly connected to both the buried channels and the thinner part of the hemipelagic layer, and supply gas to the pockmarks. Alternatively or in combination with the small-scale pathways, lateral gas transport may take place within the more permeable sandy-layers.

4.3. Molecular and Isotopic Compositions of the Hydrate-Bound Gases

Table 2 summarizes the composition of the hydrate-bound gases. Methane is overwhelmingly present and represents 99.62 mol % of the gas mixture. Ethane and carbon dioxide represent 0.02 and 0.36 mol %, respectively. Such molecular composition is similar to that measured from a hydrate-bearing pockmark nearby [Ruffine *et al.*, 2013]. The $\delta^{13}\text{C}$ -CH₄ values for methane, ethane and carbon dioxide are of -50.5 , -34 and -3 ‰, respectively. The $\delta^{13}\text{D}$ -CH₄ value for methane is of -182 ‰.

Table 2. Composition of the Hydrate-Bound Gases

| Components | Mole % | $\delta^{13}\text{C}$ (‰ PDB) | δD (‰ SMOW) |
|----------------|--------|-------------------------------|---------------------------|
| Methane | 99.62 | -50.5 | -182 |
| Ethane | 0.02 | -34.0 | |
| Carbon dioxide | 0.36 | -3.0 | |

4.4. Pore-Water Geochemistry

For all cores, chloride concentrations are constant (Figure 5) with values close to that of seawater (~560 mM), excepted for cores GMCS-12, GMMB-05, and GMMB-09 for which the concentration values were scattered at the hydrate-bearing intervals. There, they exhibit strong negative

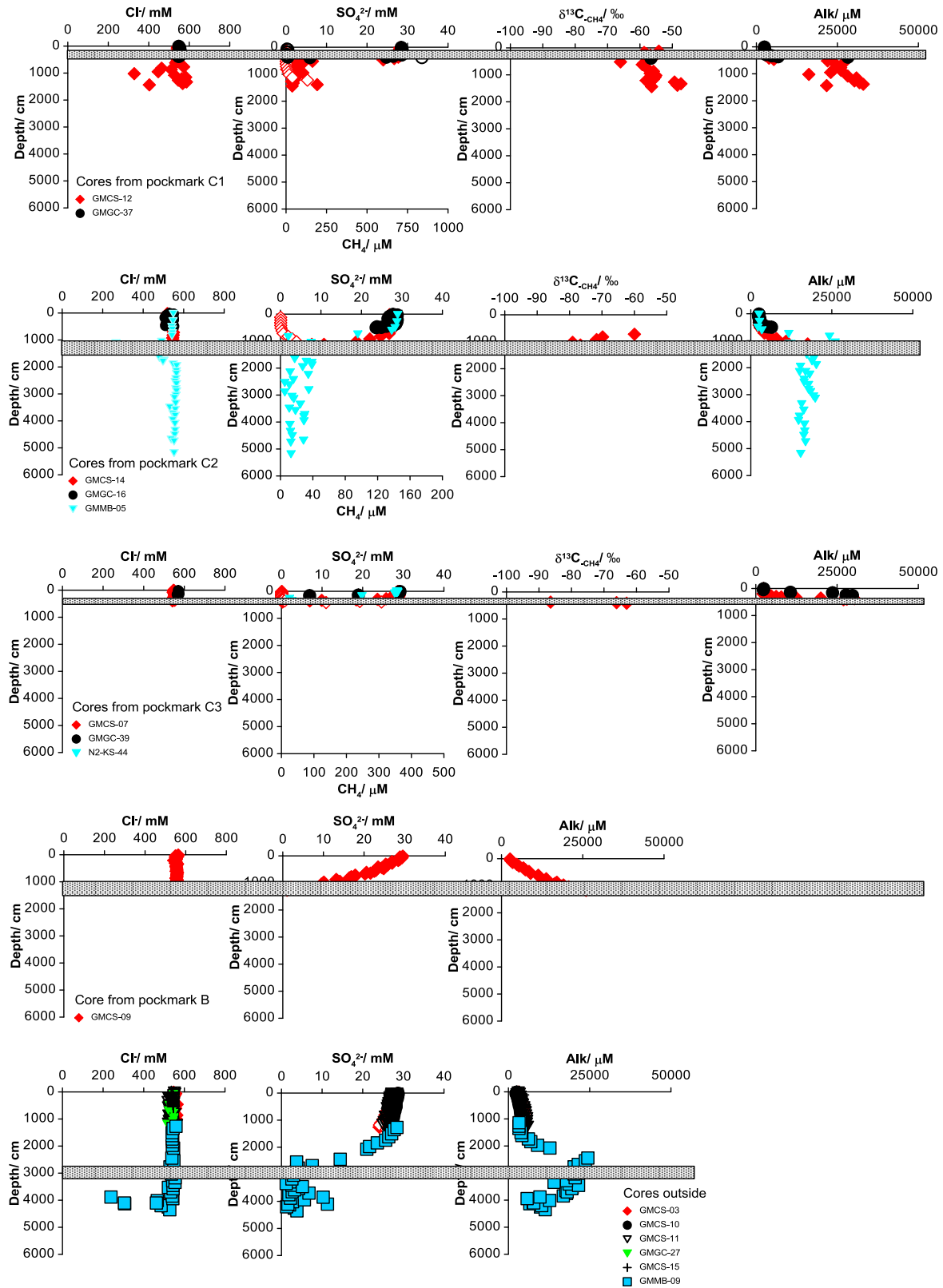


Figure 5.

concentration anomalies with values as low as 239 mM. Dissolved hydrocarbons heavier than methane were not detected in any pore-water sample. The depth concentration profiles of sulfate and methane, as well as total alkalinity are also shown in Figure 5. Sulfate concentrations and alkalinity below the SMTZ are scattered for the MeBo cores. Values of sulfate concentration higher than 0.5 mM are likely due to seawater pollution. However, correction was not made due to the difficulty to estimate the contribution of pore-water-freshening due to hydrate dissociation and seawater admixture. All gravity and Calypso cores from outside the cluster, together with the one recovered at its center, display nearly vertical and linear trends for the depth-concentration profiles for sulfate and total alkalinity, and methane concentrations do not reach the instrument detection limit ($< 0.5 \mu\text{mol L}^{-1}$). In contrast, all cores collected within the pockmarks, together with the MeBo core GMMB-09 retrieved outside, exhibit kink-type sulfate profiles [Hensen *et al.*, 2003] with two distinct segments delimited by a salient change in the concentration gradient (Figure 5); except for GMCS-09 retrieved from pockmark B and which is characterized by a slightly concave up profile. Unlike linear profiles that indicates a steady-state condition, the kink-type profiles reflect a transient-state condition resulting from changes in the methane flux [Fischer *et al.*, 2013; Hensen *et al.*, 2003]. The upper segment of the profile represents the sulfate diffusion gradient before the change in the methane flux, and the lower segment with a more important sulfate-depletion gradient implied an increase in the methane flux. The sulfate and alkalinity profiles mirror each other. Methane concentrations significantly increase with depth from the sulfate-depleted horizon (Figure 5), while $\delta^{13}\text{C}_{\text{CH}_4}$ decrease progressively with depth from -57‰ to $\leq -86\text{‰}$ for cores GMCS-14 and GMCS-07 and remains at around -57‰ for core GMCS-12.

4.5. Chemical Analysis of the Oil Sample

The whole oil GC analysis of the standard oil NSG-NSO-1 (NIGOGA) and the oil sampled from core GMCS-09 shows that hydrocarbons with less than 12 carbon atoms (C12) are not detected from our sample although those compounds are usually ubiquitous in oil (chromatogram shows in supporting information Figure S1). Furthermore, the GC \times GC analysis revealed that n-alkanes are nearly absent in our sample (see supporting information Figure S2). The different fraction TS, TA, TR, and TAs represent 35.3, 24.2, 18.4, and 0.6 mass % of the initial weight (~ 245.7 mg), respectively.

5. Discussion

5.1. Hydrocarbon Origin

Both molecular and isotopic compositions of gas are the two fundamental properties used to discuss their origin [Bernard *et al.*, 1978; Schoell, 1983; Whiticar, 1999]. Thermogenic gases are usually defined as a mixture for which the C_{2+} fraction is in a significant amount, whereas microbial gases are very dry, i.e., with a very small amount of hydrocarbons other than methane. Microbial gases result usually from microbial processes at shallow sedimentary depth which leads to ^{13}C -depleted methane [Whiticar *et al.*, 1986]. Conversely, thermogenic gases are generated at deep depth by thermal cracking of kerogen, and the resulting methane is isotopically heavier ($\delta^{13}\text{C} > \sim -50\text{‰}$). When referring to the criteria of classification defined by Bernard *et al.* [1978] shown in Figure 6a, the hydrate-bound methane and ethane fall within the thermogenic domain. The contribution of a thermogenic source of hydrocarbons is supported by the presence of oil in core GMCS-09, which clearly reflects an upward migration of thermogenic hydrocarbons. The gas dryness may then result from a diffusion-driven migration from deep-seated reservoirs [Prinzhofer and Pernaton, 1997]. However, the diffusion-driven migration hypothesis has been discarded as we will show below that gases were transported to the hydrate-bearing layers mainly by advection. On the other hand, the diagram in Figures 6b indicates that the hydrate-bound gases are a mixture of both thermogenic and microbial gases while the one in Figure 6c shows that methane falls at the boundary of the thermogenic domain and the

Figure 5. Pore-water profiles of chloride (Cl^-), sulfate (SO_4^{2-}), methane (CH_4) and alkalinity (Alk) for the investigated cores: (a) Row 1 corresponds to cores retrieved from pockmark-C1; (b) Row 2 corresponds to cores retrieved from pockmark-C2; (c) Row 3 corresponds to cores retrieved from pockmark-C3; (d) Row 4 corresponds to cores retrieved from pockmark-B; (e) Row 5 corresponds to cores retrieved outside the pockmarks. For each row, the hollow symbols of the second graph indicate methane concentrations when they were measured, whereas filled symbols correspond to sulfate concentrations. They gray line corresponds to the SMTZ. All cores showing sedimentary strata far below the SMTZ exhibit chloride profiles with negative anomalies (values lower than that of seawater) due to pore-water freshening by gas hydrate dissociation. Sulfate concentrations and alkalinity below the SMTZ are scattered for the MeBo cores. Values of sulfate concentration higher than 0.5 mM are likely due to seawater pollution. However, correction was not made due to the difficulty to quantify the contribution of pore-water-freshening due to hydrate dissociation and seawater admixture.

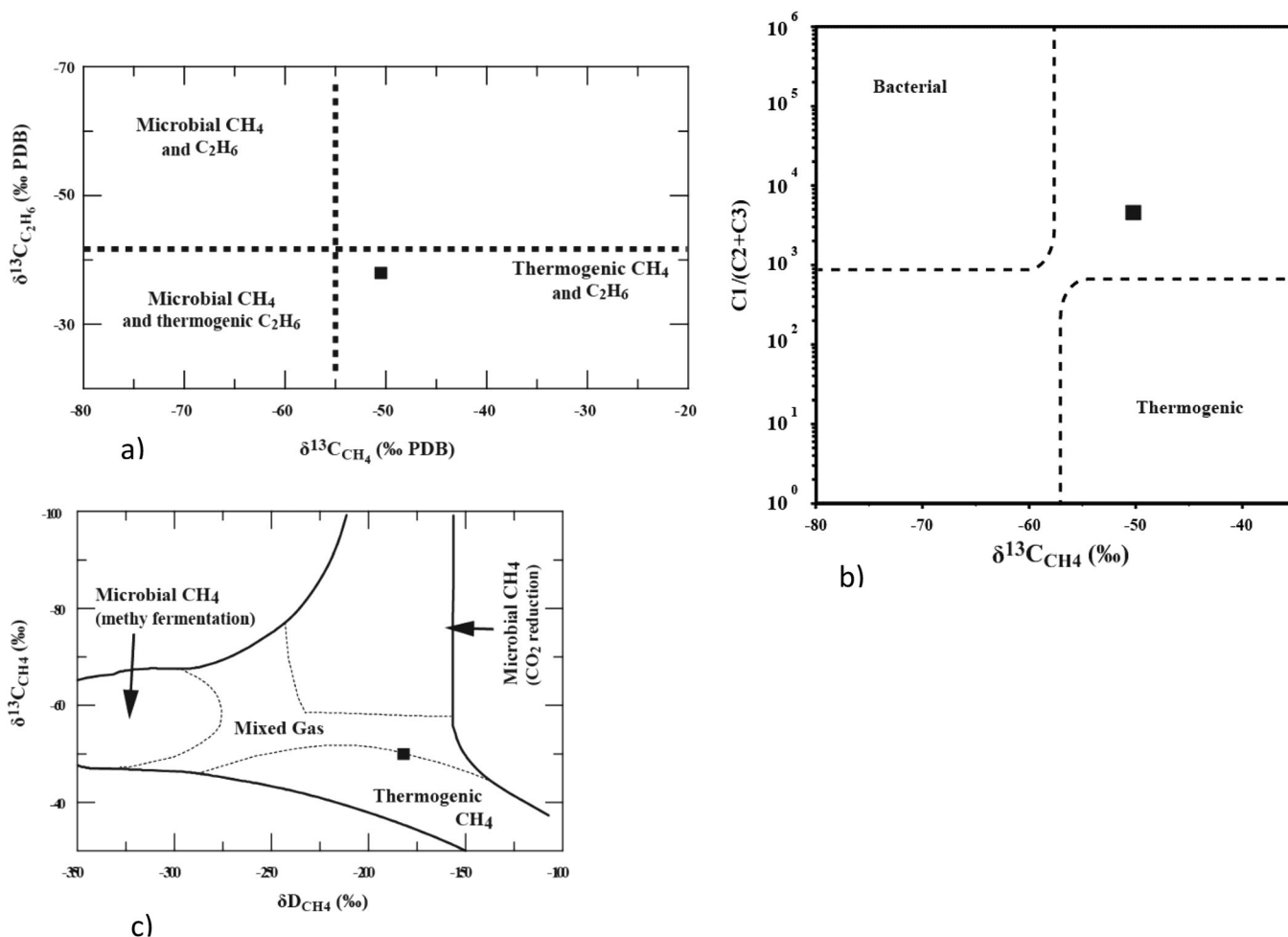


Figure 6. Geochemistry of the hydrate-bound gases: (a) Diagram of $\delta^{13}\text{C}\text{-C}_2\text{H}_6$ vs. $\delta^{13}\text{C}\text{-CH}_4$, (modified after Bernard, 1978). (b) Diagram of $\text{C}_1/\text{C}_2+\text{C}_3$ vs. $\delta^{13}\text{C}\text{-CH}_4$. (c) Diagram of $\delta^{13}\text{C}\text{-CH}_4$ and $\delta\text{D}\text{-CH}_4$ (modified after Schoell, 1983 and Whiticar, 1999).

mixed gas. Thus, the admixture of microbial gases into a thermogenic source can explain the dryness observed. In fact, Figure 5 presents very ¹³C-depleted dissolved methane with increasing values from $\leq -86\text{‰}$ to -57‰ when moving from the SMTZ to the seafloor for core GMCS-14. This suggests a removal of ¹³C-depleted dissolved methane from a microbial methane pool by the AOM followed by diffusion of the generated ¹³C-enriched dissolved methane towards the seafloor.

Thus, we believe that the gases supplying the hydrate interval, which hereby is referred to the Gas Hydrate Occurrence Zone (GHOZ), is a mixture of a thermogenic and microbial gases. The thermogenic sources are likely the identified hydrocarbon-charged bodies at deep depths in Figure 4.

5.2. Hydrocarbon Migration Pattern into the Sedimentary Column

The sulfate-diffusion profiles observed for cores GMGC-27, GMCS-10, GMCS-11, and GMCS-15 as well as the absence of hydrocarbons measured in the collected pore-water samples indicate that hydrocarbon migration is not taking place within the upper ten of meters of sedimentary column outside the depressions. Furthermore, the SYSIF seismic surveys indicate that gas hydrates are present in the surficial sedimentary column only within the cluster Pockmark-C, and one can clearly see in Figures 2 and 3 that the hydrate-bearing sedimentary intervals are shallower at the center and deeper when moving away to the rim. These results are in agreement with the geochemical results from the sequence of cores collected along those profiles (Figure 1b). The depths of the amplitude anomalies encountered along these profiles coincide perfectly with the intervals where gas hydrates were recovered. Based on the visual observation of hydrates and the development of negative anomalies from the chloride profiles of cores GMCS-12, GMMB-05 and

GMMB-09 (Figure 5) due to pore-water freshening upon hydrate dissociation [Hesse and Harrison, 1981; Torres et al., 2004], shallow gas hydrates were located from around 7.7 and 15–20 mbsf within pockmark-C1 and pockmark-C2, respectively, and from 38.5 mbsf outside [Wei et al., 2015]. The recovered hydrates were porous, with a honeycombed aspect [Sultan et al., 2014]. This observation combined with the coexistence of free gas within the GHZO suggest a rapid hydrate formation within the sedimentary column from free gas transported by advection, with gas bubbles trapped within the hydrate fabric. On the opposite, gas hydrates have not been sampled in pockmark B as the length of core GMCS-09 was not long enough to reach the sedimentary section below the SMTZ. However, the VHR seismic profile in Figure 2 does not show any acoustic shadow indicative of their occurrence. Thus, it is clear that the GHZO within the cluster Pockmark-C are the major shallow gas reservoir in the area. Conversely, the presence of authigenic carbonate concretions from 5.75 to 12.45 mbsf along the entire length of core GMCS-09 is indicative of the past gas-migration activity of pockmark-B, which latter has been replaced by oil migration. Thus, these results clearly demonstrate that shallow hydrocarbon-migration is exclusively restricted to within the pockmarks, and is in agreement with several studies from other settings [Cathles et al., 2009; Chand et al., 2009; Hovland et al., 2010; León et al., 2010; Macelloni et al., 2012; Ostanin et al., 2013; Simonetti et al., 2013; Sultan et al., 2010; Sun et al., 2011]. Moreover, although the geological system here is different from that observed in Woolsey Mound in the Gulf of Mexico where the fault system was generated from salt tectonic movement [Macelloni et al., 2012; Simonetti et al., 2013], there are some similarities. Especially, the fractures created from gas accumulation followed by discharge act alternatively as gas conduits and hydrate traps.

5.3. Sulfate Reduction Within the Pockmark Cluster: Constraining the Time of Hydrate-Layer Formation Within the Pockmarks and Outside

On continental margins, the two major processes responsible for sulfate depletion in pore waters are the Organoclastic Sulfate Reduction (OSR) [Claypool and Kaplan, 1974; Malinverno and Pohlman, 2011] and the Anaerobic Oxidation of Methane (AOM) [Boetius et al., 2000; Reeburgh, 1976]. Dissolved methane concentrations from the Calypso cores recovered outside the pockmarks are below the detection limit, suggesting that CH₄ is not present in the near-surface sediment or eventually present at small amount. This is also the case for the upper part of the MeBo core GMMB-09. Thus, AOM does not significantly occur at the surficial sediment outside the pockmarks. In addition, the sulfate profiles of the same cores display concentrations close to that of seawater. This indicates that OSR is not significantly occurring outside the pockmarks neither, or alternatively any sulfate consumption is cancelled out by a quick resupply from the overlying seawater. Because the sulfate profiles of the cores collected within the pockmarks are also characterized by seawater-like concentration values over their first meters depth and gas plumes have not been detected from the acoustic survey of the water column over the cluster, it is likely that OSR is also not significant within the depressions. Such low sulfate reduction rate over meter scale within the sedimentary column has already been observed in pockmark fields of the SW-Barents Sea [Nickel et al., 2012].

Accordingly, AOM is the only process responsible for the sulfate depletion within the pockmarks and the methane is come from the GHZO. In fact, as shown in Figure 5, the combination of total alkalinity, sulfate and methane concentrations, together with $\delta^{13}\text{C-CH}_4$ for all cores collected within the hydrate-bearing pockmarks, consistently display the evidence of AOM. The AOM reaction consumes sulfate and methane at the SMTZ, and releases bicarbonate ions. The total depletion of sulfate and a maximum in alkalinity concentration at the SMTZ explains the reciprocal trend observed for the profiles of these species [Chatterjee et al., 2011; Kastner et al., 2008; Ruffine et al., 2015].

When approaching the SMTZ, $\delta^{13}\text{C-CH}_4$ values reach -86‰ for cores GMCS-07 and GMCS-14, which is within typical values usually found at methanogenic horizon [Whiticar, 1999; Yoshinaga et al., 2014]. However, the $\delta^{13}\text{C-CH}_4$ of core GMCS-12 is very scattered, with all values centered around -57‰ . This likely results from the mixing of the hydrate-bound methane having a $\delta^{13}\text{C-CH}_4$ value of -50.5‰ with much lighter methane generated at the methanogenic zone beneath the SMTZ. In the case of pockmark-B, oxidation of hydrocarbons heavier than methane may also be responsible for the sulfate depletion. This is supported by chemical analysis of the oil sample where saturated fraction TS is rather low (35.3%- mass); and confirmed by the lack of n-alkanes in the oil sample (see supporting information Figure S2). In fact, microbial-mediated oil degradation consumes preferentially the n-alkanes [Dimitrakopoulos and Muehlenbachs, 1987; Head et al., 2003; Jones et al., 2007], and thus the degraded oil is enriched with the other fractions.

Table 3. Depth of the SMTZ for the Investigated Cores

| Location in the Cluster | Core Name | SMTZ Depth |
|--------------------------------|-----------|------------|
| Pockmark B | GMCS-09 | 12.7 |
| Pockmark C1 | GMCS-12 | 6.2 |
| Pockmark C1 | GMGC-37 | 4 |
| Pockmark C2 | GMCS-14 | 14 |
| Pockmark C2 | GMCS-16 | 6 |
| Pockmark C2 | GMMB-05 | 11.2 |
| Pockmark C3 | GMCS-07 | 3.7 |
| Pockmark C3 | GMGC-39 | 1.8 |
| Pockmark C3 | N2-KS-44 | 2.7 |
| Outside, center of the cluster | GMGC-27 | |
| Outside | GMMB-09 | 33.4 |
| Outside | GMCS-03 | |
| Outside | GMCS-10 | |
| Outside | GMCS-11 | |
| Outside | GMCS-15 | |

As mentioned above, the kink-type sulfate profiles observed for all cores presenting evidence of AOM is representative of systems at transient state [Fischer *et al.*, 2013; Hensen *et al.*, 2003; Noethen and Kasten, 2011]. Table 3 shows that the SMTZ depth differs according to the core location; even within the same pockmark. As expected, the shallowest SMTZ depths are encountered above the shallowest hydrate-bearing intervals, and the deepest one has been found for core GMCS-14 located close to the rim of pockmark-C2, at 14 mbsf. Recent studies in this area show that gas hydrates were distributed as layered fronts within the sedimentary column (also observed from Figures 2 and 3) and result from episodic release of gas followed by fast formation [Sultan *et al.*, 2014;

Wei *et al.*, 2015], and there is a linear relationship between the depths of the SMTZ and the top of the GHZOZ [Bayon *et al.*, 2015]. Based on the pockmark evolution scheme proposed by Sultan *et al.* [2014], we estimated the elapsed times for the formation of the uppermost sampled hydrate layers for each hydrate-bearing pockmark as well as outside the cluster by simulating the evolution of the sulfate profile over time for four selected cores using the transport- reaction model.

For the simulation, the following assumptions were made:

1. The formation of the hydrate layers was rapid as mentioned previously. This is supported by the coexistence of free gas and hydrates within the GHZOZ, as well as the porous aspect of the hydrate fabric.
2. Prior to the hydrate formation, methane was not present to allow the establishment of AOM within the uppermost sedimentary column and OSR is not significant. This is supported by the linear upper segment of the sulfate profiles with concentrations very close to that of seawater.
3. AOM is the only reaction leading to the depletion of sulfate, the hydrate layer is the only methane source for this reaction, and gas-hydrate dissolution is the only process which supplies methane to the AOM. This is supported by the lack of gas plume observed at the pockmark cluster.
4. Both methane and sulfate are transported by diffusion. This is supported by the linear sulfate gradient observed at the upper part of the sulfate profiles.

The simulation results are presented in Figure 7 and summarized in Table 4. Sedimentation rates are smaller than 0.21 mm yr^{-1} in the area [Bayon *et al.*, 2015], and this maximum value has a negligible impact on the model results suggesting that fluids are not buried during this process. The time for the hydrate-layer formation varies significantly with the depth of the layer. Outside the pockmark, where the sampled hydrate-layer is located at ~ 38.5 mbsf for core GMMB-09, a formation age of around 3750 ± 250 years is found. Within the depressions, the calculated elapsed time since the hydrate-layer formation is in the order to 80 ± 10 , 1420 ± 70 , and 21 ± 2 years for GMCS-12 from pockmark-C1, GMCS-14 from pockmark-C2 and GMCS-07 from pockmark-C3, respectively. The provided accuracy is based on a sensitivity analysis for k_{AOM} and the length of the definition domain (Figure 8 shows the results for core GMCS-12). The variation of the reaction rate impacts on the thickness of the SMTZ [Chuang *et al.*, 2013]. Figure 7a shows that the SMTZ changes less than 0.5 m thick for k_{AOM} values ranging between 0.32 and $3.2 \text{ mM}^{-1} \text{ yr}^{-1}$. Values in the same order of magnitude have been found for other hydrate-bearing or gassy settings [Chatterjee *et al.*, 2011; Chuang *et al.*, 2013; Fischer *et al.*, 2013; Mogollon *et al.*, 2012; Schmidt *et al.*, 2005; Wallmann *et al.*, 2006]. The model results are more sensitive to the domain length. As mentioned previously, the latter was constrained by geochemical and geophysical considerations. Figure 7b presents the results when running the model over 80 years for a variation of $\pm 10\%$ of the domain length. The profiles obtained with the domain lengths of 7 and 7.7m are comparable. A domain length of 8.4m leads to a deeper SMTZ depth located at 6.9 mbsf instead of 6.2 mbsf. The best fit is obtained after 120 years (profile not shown), and we believe that this value remains reasonable although outside the accuracy range.

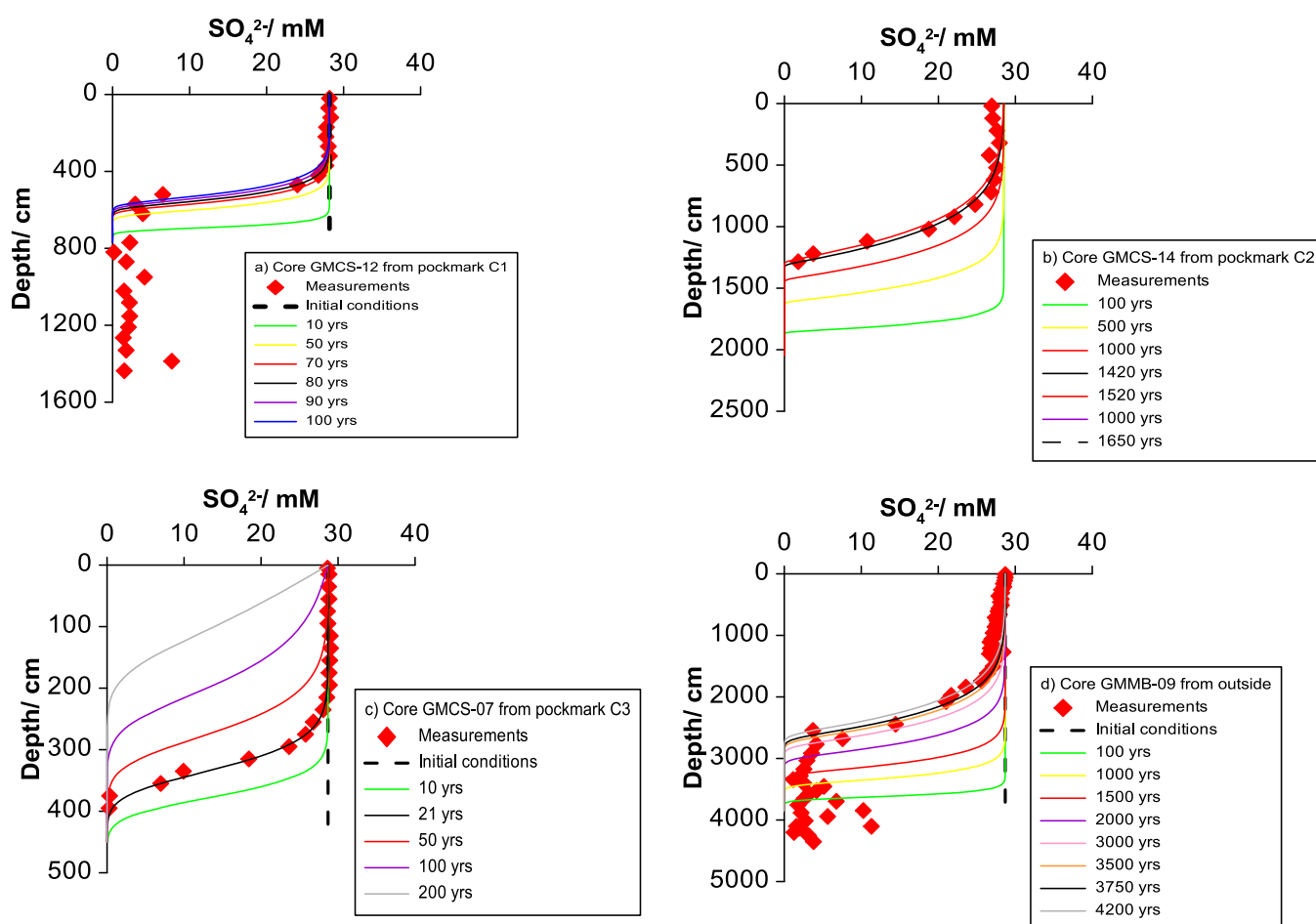


Figure 7. Evolution of the sulfate profile over time for the three hydrate-bearing pockmarks where the SMTZ: (a) Core GMCS-12 from Pockmark-C1; (b) Core GMCS-14 from Pockmark-C2; (c) Core GMCS-07 from Pockmark-C3; (d) Core GMMB-09 from outside. The model assumes that the sulfate profile starts evolving from the establishment of the hydrate layer. The results indicate that the hydrate layers supplying methane to the AOM were formed between around 20 and 4000 years ago.

As one can expect, the youngest hydrate layers correspond to the shallowest as well. The youngest formation ages are in the same order of magnitude of estimates for gas release followed by hydrate-layer formation off Pakistan [Fischer *et al.*, 2013] at similar GHOZ depths. Thus, these results indicate that the hydrate-bearing pockmarks have undergone recent hydrate formation fronts, and this is clearly confirmed by the chloride concentrations reaching 604 mM for several cores (Figure 5); whereas the background value is of ~ 550 mM. This is further supported by results from core GMMB-04 collected in pockmark-C2 where chloride concentrations are as high as 682 mM [Wei *et al.*, 2015]. Such positive chloride anomalies are indicative of recent hydrate formation [Haeckel *et al.*, 2004; Torres *et al.*, 2004], and have already been observed in the area [Ruffine *et al.*, 2013]. Hydrates were neither collected nor inferred in Pockmark-B. The widespread occurrence of carbonate concretions indicates a much older depression compared to the cluster Pockmark-C.

Considering a sedimentation rate of 0.2 mm yr^{-1} [Bayon *et al.*, 2015] and the 60-m thickness of homogeneous sedimentary cover (Figure 2), an estimated burial age of 300 kyrs B. P. is found for Pockmark B.

5.4. Link Between Fluid Flow, Surface Morphology, and Pockmark Dynamics

In the previous sections, we have shown that (1) oil is present only within pockmark B, (2) dissolved methane is present in the shallow sedimentary layers only within the cluster Pockmark-C, (3) the deepest SMTZ depths are found close to

Table 4. Model Results for the Sulfate-Profiles Evolution With Time

| Core Name | Top of the Hydrate Layer | Time Elapsed to Reach Present-Day Profile/yr |
|-----------|--------------------------|--|
| GMCS-12 | 7.7 | 80 ± 10 |
| GMCS-14 | 20.5 | 1420 ± 70 |
| GMCS-07 | 4.5 | 21 ± 2 |
| GMMB-09 | 38.5 | 3750 ± 250 |

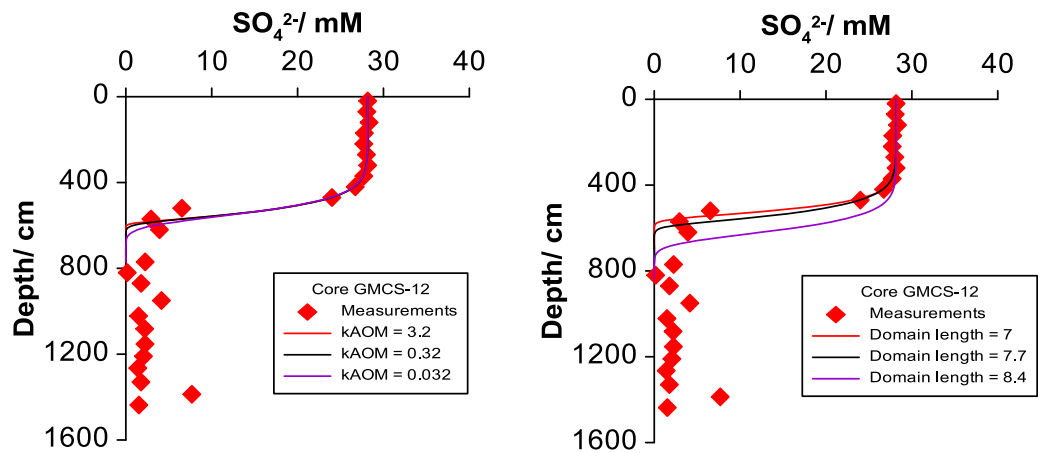


Figure 8. Sensitivity analysis for (a) the model parameter k_{AOM} and (b) the domain length.

the rim of the pockmark, while the shallowest ones are found near their center. Overall, one can clearly see that the shallowest SMTZ depths are encountered at sites characterized by positive reliefs and where the GHZO is shallow (Figures 1 to 3). In addition, the fact that shallow hydrates were recovered at the bulges suggests that the hydrate formation induced an uplift of the superficial sediment as observed on the Eastern Margin of the Japan sea [Freire et al., 2012]. These observations combined with the high contrast in

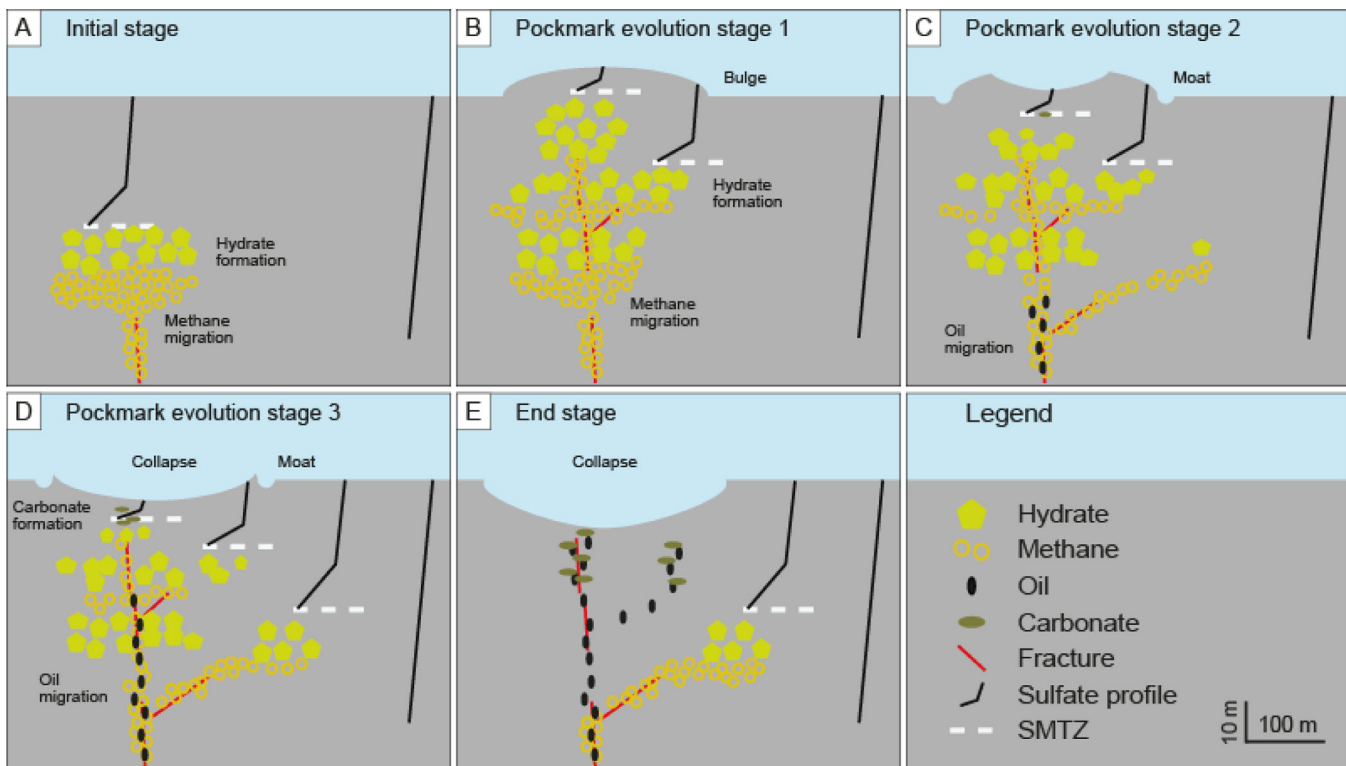


Figure 9. Conceptual representation of the influence of fluid flow on the evolution of hydrate-bearing pockmarks off Nigeria: (a) and (b) The presence of massive hydrates at depth does not impact on the surface sediment as observed from MeBo core GMMB-09 collected outside the pockmarks. Rapid formation of the hydrate layer with a low permeability allow gas to accumulate within the GHZO and beneath. This results in an overpressure of the sediment, creating faults or fractures through which gas migrates upwardly to form a new hydrate layer at shallowest depth. If the layer is close to the seabed, the hydrate formation induces a deformation of the surface sediment by forming positive relief like bulges as observed on pockmark-C1 and pockmark-C3 where the shallowest layers were sampled. (c) The GHZO starts shrinking as it supplies methane to the AOM reaction, leading to the collapse of the bulges to moats as observed on pockmark-B, the western part of pockmark-C2 and the northern part of pockmark-C3. (d) and (e) The AOM, in turn, produces carbonate ions which favor the precipitation of solid carbonates. Over time, the GHZO disappears if there is no gas supply to balance the hydrate dissolution; and oil migration follows as observed for pockmark-B.

shape of the sulfate profiles for cores GMCS-14 and GMCS-15, two cores located close to each other with the former being within Pockmark-C2 and the latter outside, strongly highlight the links between fluid flow, gas hydrate occurrence and pockmark perimeter and morphology at the investigated area. They definitely prove that hydrocarbon migration plays an important role in the establishment of the rim of pockmarks. In Figure 9, we proposed a conceptual model to illustrate the link between fluid flow and pockmark evolution at the study area: The presence of massive hydrates at depth does not affect the surface sediment as observed from MeBo core GMMB-09 collected outside the pockmarks (Figures 9a and b). Because of the low permeability of the hydrates and their rapid formation at this site, gas is allowed to accumulate within the GHZO and beneath. This results in an overpressure of the sediment, creating faults or fractures through which gas migrates upwardly to form a new hydrate layer at shallowest depth. A similar mechanism alternating between fluid flow and hydrate formation at fractures has been proposed at Woolsey Mount in Northern Gulf of Mexico [Macelloni *et al.*, 2012; Simonetti *et al.*, 2013]. However, in the case of the Woolsey Mount, fractures were generated by the upward movement of a salt body. Here, the extracted line from the 3D industry seismic (Figure 4) show neither salt body beneath the depressions nor master faults acting as direct gas conduits connected to the depressions. Providing that the hydrates precipitate close enough to the seabed, the resulting hydrate layers induce its deformation by forming positive reliefs like bulges as observed on pockmark-C1 and pockmark-C3 where the shallowest layers were sampled. The gas hydrate occurrence zone starts shrinking as it supplies methane to the AOM reaction (Figure 9c). This leads to the collapse of the bulges to moats as observed on pockmark-B, the western part of pockmark-C2 and the northern part of pockmark-C3. The AOM, in turn, produces carbonate ions, which favor the precipitation of solid carbonates (Figure 9d). Over time, the GHZO disappears if there is not enough gas supply to balance the hydrate dissolution and oil migration follows as observed for pockmark-B as its density is higher (Figure 9e). In the proposed scenario, we assume a change in the hydrocarbon migration from gas to oil with the temporal evolution of the pockmark and such an evolution has not been reported elsewhere. However, Figure 10 represents a section of core GMCS-09 where the oil is mostly located around the carbonate concretions. The same pattern is found for all core sections. Thus, one might assume that the carbonates favor the

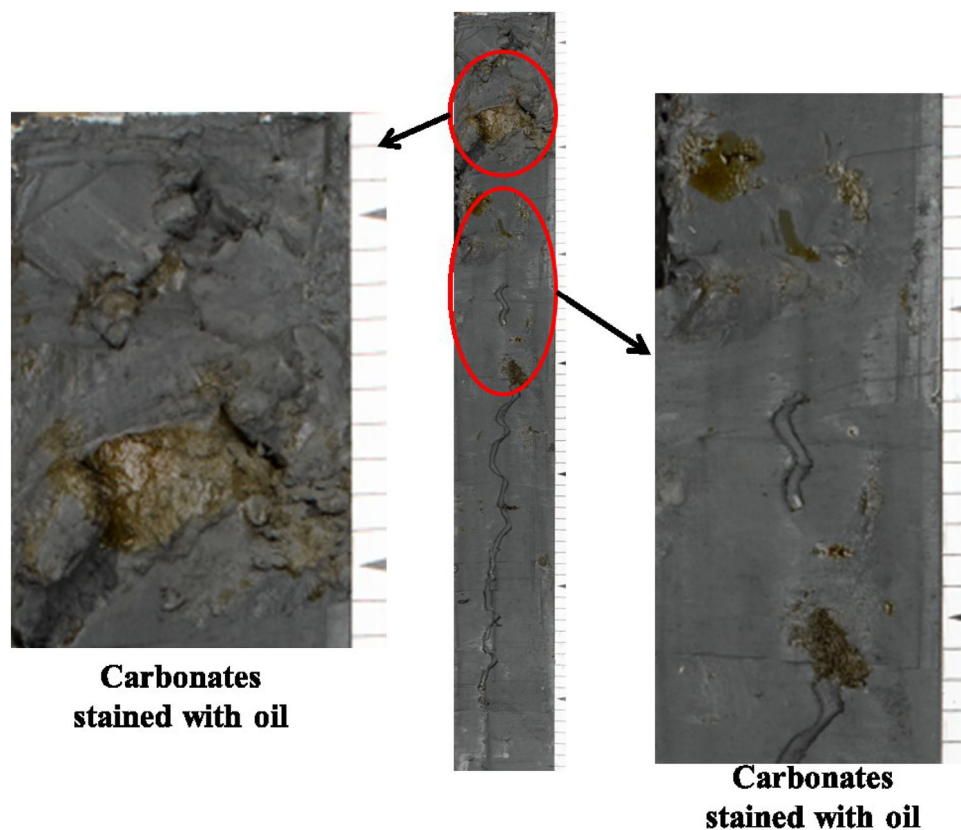


Figure 10. Section of core GMCS-09 collected on pockmark-B: Oil is mainly distributed at the locations where carbonates are found.

oil migration and this would explain their occurrences only in the shallow sediment of pockmark-B. However, the study of the evolution of the sediment permeability with the precipitation of authigenic carbonates is needed to verify our hypothesis.

6. Conclusion

Four pockmarks off Nigeria have been consistently sampled along pre-determined seismic lines and at key locations in order to better understand both the fluid flow pattern and hydrate layer distribution over that cluster. The combination of *in situ* sample-based geochemical analyses with AUV bathymetry and seismic data reveals that:

- The hydrocarbon source supplying the cluster is a mixture of both thermogenic and microbial sources.
- Shallow hydrocarbon migration (depth $< \sim 30$ mbsf) is focused only within the pockmarks. While gas migration takes place within the hydrate-bearing pockmarks, the carbonate-rich pockmark is characterized by oil migration.
- The short distance between the SMTZ and the GHZ supports for a hydrate dissolution process driven by AOM.

A numerical transport-reaction model was developed to estimate the hydrate-layer formation time into the sedimentary column. The results showed that the oldest and deepest hydrate layer is located outside the pockmark and has been formed ~ 3750 years ago, while the latest one was formed ~ 21 years ago. Thus, the modeling results demonstrate that the hydrate-bearing pockmark cluster has been active for at least 3750 years, and the positive anomalies observed from the chloride profiles indicate that it is still in a stage dominated by hydrate formation. The burial of the carbonate-rich pockmark started ~ 300 kyrs ago.

Overall, this study further supports the important role of fluid flow on pockmark dynamics. Our findings may have implications for the offshore hydrocarbon production as it shows that sudden releases of gas can create hydrate layers within the upper sedimentary column that can affect the seafloor morphology over few decades. Thus, such considerations need to be taken into account in the assessment of sites to accommodate offshore-production installations of hydrocarbons of similar lifespan.

Acknowledgments

We thank all the crew on-board the *RV Pourquoi pas?* as well as the MeBo crew for their technical support. We express our gratitude to Dr. Marsset Bruno for valuable suggestions and comments regarding the seismic data. We also gratefully acknowledge the reviewers for their constructive criticisms. Data used in the present paper are covered by a confidentiality agreement between Total, IFREMER and Marum that restrict access; interested readers can contact the corresponding author for more information (livio.ruffine@ifremer.fr).

References

- Alberto, M., J. Arah, H. Neue, R. Wassmann, R. Lantin, J. Aduna, and K. Bronson (2000), A sampling technique for the determination of dissolved methane in soil solution, *Chemosphere-Global Change Sci.*, 2(1), 57–63.
- Andresen, K. J., M. Huuse, and O. Clausen (2008), Morphology and distribution of Oligocene and Miocene pockmarks in the Danish North Sea—implications for bottom current activity and fluid migration, *Basin Res.*, 20(3), 445–466.
- Bayon, G., G. M. Henderson, J. Etoubleau, J.-C. Caprais, L. Ruffine, T. Marsset, B. Dennielou, E. Cauquil, M. Voisset, and N. Sultan (2015), U-Th isotope constraints on gas hydrate and pockmark dynamics at the Niger delta margin, *Mar. Geol.*, 370, 87–98.
- Bernard, B. B., J. M. Brooks, and W. M. Sackett (1978), Light-hydrocarbons in recent Texas continental-shelf and slope sediments, *J. Geophys. Res.*, 83, 4053–4061.
- Berndt, C. (2005), Focused fluid flow in passive continental margins, *Philos. Trans. R. Soc. A Math. Phys. Eng. Sci.*, 363(1837), 2855–2871.
- Berner, R. (1980), *Early Diagenesis: A Theoretical Approach*, Princeton Univ. Press, Princeton, N. J.
- Betzler, C., S. Lindhorst, C. Huebscher, T. Luedmann, J. Fuerstenau, and J. Reijmer (2011), Giant pockmarks in a carbonate platform (Maldives, Indian Ocean), *Mar. Geol.*, 289(1–4), 1–16.
- Bilotti, F., and J. H. Shaw (2005), Deep-water Niger Delta fold and thrust belt modeled as a critical-taper wedge: The influence of elevated basal fluid pressure on structural styles, *AAPG Bull.*, 89(11), 1475–1491.
- Boetius, A., K. Ravensschlag, C. J. Schubert, D. Rickert, F. Widdel, A. Gieseke, R. Amann, B. B. Jorgensen, U. Witte, and O. Pfannkuche (2000), A marine microbial consortium apparently mediating anaerobic oxidation of methane, *Nature*, 407(6804), 623–626.
- Boudreau, B. (1997), *Diagenetic Models and their Implementation*, 1st ed., 414 pp., Springer-Verlag, Berlin.
- Burke, K. (1972), Longshore drift, submarine canyons, and submarine fans in development of Niger Delta, *Am. Assoc. Pet. Geol. Bull.*, 56(10), 1975–1983.
- Cathles, L. M., Z. Su, and D. F. Chen (2009), The physics of gas chimney and pockmark formation, with implications for assessment of seafloor hazards and gas sequestration, *Mar. Pet. Geol.*, 27(1), 82–91.
- Chand, S., L. Rise, D. Ottesen, M. F. J. Dolan, V. Bellec, and R. Bøe (2009), Pockmark-like depressions near the Goliath hydrocarbon field, Barents Sea: Morphology and genesis, *Mar. Pet. Geol.*, 26(7), 1035–1042.
- Chatterjee, S., G. R. Dickens, G. Bhatnagar, W. G. Chapman, B. Dugan, G. T. Snyder, and G. J. Hirasaki (2011), Pore water sulfate, alkalinity, and carbon isotope profiles in shallow sediment above marine gas hydrate systems: A numerical modeling perspective, *J. Geophys. Res.*, 116, B09103, doi:10.1029/2011JB008290.
- Chen, S.-C., S.-K. Hsu, C.-H. Tsai, C.-Y. Ku, Y.-C. Yeh, and Y. Wang (2010), Gas seepage, pockmarks and mud volcanoes in the near shore of SW Taiwan, *Mar. Geophys. Res.*, 31(1–2), 133–147.

- Chuang, P.-C., et al. (2013), Relating sulfate and methane dynamics to geology: Accretionary prism offshore SW Taiwan, *Geochem. Geophys. Geosyst.*, *14*, 2523–2545, doi:10.1002/ggge.20168.
- Claypool, G. E., and I. R. Kaplan (1974), The origin and distribution of methane in marine sediments, in *Natural Gases in Marine Sediments*, edited by I. R. Kaplan, pp. 99–139, Plenum, New York.
- Cohen, H. A., and K. McClay (1996), Sedimentation and shale tectonics of the northwestern Niger Delta front, *Mar. Pet. Geol.*, *13*(3), 313–328.
- Corredor, F., J. H. Shaw, and F. Bilotti (2005), Structural styles in the deep-water fold and thrust belts of the Niger Delta, *AAPG Bull.*, *89*(6), 753–780.
- Damuth, J. E. (1994), Neogene gravity tectonics and depositional processes on the deep Niger-delta continental-margin, *Mar. Pet. Geol.*, *11*(3), 320.
- Davy, B., I. Pecher, R. Wood, L. Carter, and K. Gohl (2010), Gas escape features off New Zealand: Evidence of massive release of methane from hydrates, *Geophys. Res. Lett.*, *37*, L21309, doi:10.1029/2010GL045184.
- Dickens, G. R., M. Koelling, D. C. Smith, and L. Schnieders (2007), Rhizon sampling of pore waters on scientific drilling expeditions: An example from the IODP Expedition 302, Arctic Coring Expedition (ACEX), *Sci. Drill.*, *4*, 22–25.
- Dimitrakopoulos, R., and K. Muehlenbachs (1987), Biodegradation of petroleum as a source of ^{13}C -enriched carbon dioxide in the formation of carbonate cement, *Chem Geol.*, *65*(3–4), 283–291.
- Fischer, D., J. M. Mogollon, M. Strasser, T. Pape, G. Bohrmann, N. Fekete, V. Spiess, and S. Kasten (2013), Subduction zone earthquake as potential trigger of submarine hydrocarbon seepage, *Nat. Geosci.*, *6*(8), 647–651.
- Freire, A. F. M., R. Matsumoto, and F. Akiba (2012), Geochemical analysis as a complementary tool to estimate the uplift of sediments caused by shallow gas hydrates in mounds at the seafloor of Joetsu Basin, eastern margin of the Japan Sea, *J. Geol. Res.*, *2012*, 1–14.
- Gay, A. (2002), Les marqueurs géologiques de la migration et de l'expulsion des fluides sédimentaires sur le plancher des marges passives matures: exemples dans le bassin du Congo, Lille 1.
- Gay, A., M. Lopez, H. Ondreas, J. Charlou, G. Sermondadaz, and P. Cochonat (2006), Seafloor facies related to upward methane flux within a Giant Pockmark of the Lower Congo Basin, *Mar. Geol.*, *226*(1–2), 81–95.
- George, R., and E. Cauquil (2007), AUV ultrahigh-resolution 3D seismic technique for detailed subsurface investigations, paper presented at Offshore Technology Conference, 30 April–3 May, Houston, Tex.
- Haeckel, M., E. Suess, K. Wallmann, and D. Rickert (2004), Rising methane gas bubbles form massive hydrate layers at the seafloor, *Geochim. Cosmochim. Acta*, *68*(21), 4335–4345.
- Head, I., D. Jones, and S. Larter (2003), Biological activity in the deep subsurface and the origin of heavy oil, *Nature*, *426*(6964), 344–352.
- Hensen, C., M. Zabel, K. Pfeifer, T. Schwenk, S. Kasten, N. Riedinger, H. D. Schulz, and A. Boettius (2003), Control of sulfate pore-water profiles by sedimentary events and the significance of anaerobic oxidation of methane for the burial of sulfur in marine sediments, *Geochim. Cosmochim. Acta*, *67*(14), 2631–2647.
- Hesse, R., and W. E. Harrison (1981), Gas hydrates (Clathrates) causing pore-water freshening and oxygen isotope fractionation in deep-water sedimentary sections of terrigenous continental margins, *Earth Planet. Sci. Lett.*, *55*(3), 453–462.
- Ho, S., J. Cartwright, and P. Imbert (2012), The formation of advancing pockmarks arrays: An interplay between hydrocarbon leakage and slope sedimentation, paper presented at AAPG Annual Convention and Exhibition, Search and Discovery, Article 50592.
- Hovland, M., and A. Judd (1988), *Seabed Pockmarks and Seepages: Impact on Geology, Biology, and the Marine Environment*, Graham and Trotman, London, U. K.
- Hovland, M., J. V. Gardner, and A. G. Judd (2002), The significance of pockmarks to understanding fluid flow processes and geohazards, *Geofluids*, *2*(2), 127–136.
- Hovland, M., R. Heggland, M. H. De Vries, and T. I. Tjelta (2010), Unit-pockmarks and their potential significance for predicting fluid flow, *Mar. Pet. Geol.*, *27*(6), 1190–1199.
- Jones, D., I. Head, N. Gray, J. Adams, A. Rowan, C. Aitken, B. Bennett, H. Huang, A. Brown, and B. Bowler (2007), Crude-oil biodegradation via methanogenesis in subsurface petroleum reservoirs, *Nature*, *451*(7175), 176–180.
- Josenhans, H. W., L. H. King, and G. B. Fader (1978), A side-scan sonar mosaic of pockmarks on the Scotian Shelf, *Can. J. Earth Sci.*, *15*(5), 831–840.
- Judd, A. A. G., and M. Hovland (2007), *Seabed Fluid Flow: The Impact of Geology, Biology and the Marine Environment*, Cambridge Univ. Press, U. K.
- Kastner, M., G. Claypool, and G. Robertson (2008), Geochemical constraints on the origin of the pore fluids and gas hydrate distribution at Atwater Valley and Keathley Canyon, northern Gulf of Mexico, *Mar. Pet. Geol.*, *25*(9), 860–872.
- Ker, S., B. Marsset, S. Garziglia, Y. Le Gonidec, D. Gibert, M. Voisset, and J. Adamy (2010), High-resolution seismic imaging in deep sea from a joint deep-towed/OBH reflection experiment: application to a Mass Transport Complex offshore Nigeria, *Geophys. J. Int.*, *182*(3), 1524–1542.
- King, L. H., and B. MacLean (1970), Pockmarks on the Scotian shelf, *Geol. Soc. Am. Bull.*, *81*(10), 3141–3148.
- León, R., L. Somoza, T. Medialdea, F. J. Hernández-Molina, J. T. Vázquez, V. Díaz-del-Río, and F. J. González (2010), Pockmarks, collapses and blind valleys in the Gulf of Cádiz, *Geo-Mar. Lett.*, *30*(3–4), 231–247.
- Luo, M., A. W. Dale, K. Wallmann, C. Hensen, J. Gieskes, W. Yan, and D. Chen (2015), Estimating the time of pockmark formation in the SW Xisha Uplift (South China Sea) using, reaction-transport modeling, *Mar. Geol.*, *364*, 21–31.
- Macelloni, L., A. Simonetti, J. H. Knapp, C. C. Knapp, C. B. Lutken, and L. L. Lapham (2012), Multiple resolution seismic imaging of a shallow hydrocarbon plumbing system, Woolsey Mound, Northern Gulf of Mexico, *Mar. Pet. Geol.*, *38*(1), 128–142.
- Malinverno, A., and J. W. Pohlman (2011), Modeling sulfate reduction in methane hydrate-bearing continental margin sediments: Does a sulfate-methane transition require anaerobic oxidation of methane?, *Geochem. Geophys. Geosyst.*, *12*, Q07006, doi:10.1029/2011GC003501.
- Marsset, T., B. Marsset, S. Ker, Y. Thomas, and Y. Le Gall (2010), High and very high resolution deep-towed seismic system: Performance and examples from deep water Geohazard studies, *Deep Sea Res. Part I Oceanogr Res Pap.*, *57*(4), 628–637.
- Milkov, A. V., G. R. Dickens, G. E. Claypool, Y. J. Lee, W. S. Borowski, M. E. Torres, W. Y. Xu, H. Tomaru, A. M. Trehu, and P. Schultheiss (2004), Co-existence of gas hydrate, free gas, and brine within the regional gas hydrate stability zone at Hydrate Ridge (Oregon margin): Evidence from prolonged degassing of a pressurized core, *Earth Planet. Sci. Lett.*, *222*(3–4), 829–843.
- Mogollon, J. M., A. W. Dale, H. Fossing, and P. Regnier (2012), Timescales for the development of methanogenesis and free gas layers in recently-deposited sediments of Arkona Basin (Baltic Sea), *Biogeosciences*, *9*(5), 1915–1933.
- Moss, J., J. Cartwright, and R. Moore (2012), Evidence for fluid migration following pockmark formation: Examples from the Nile Deep Sea Fan, *Mar. Geol.*, *303*, 1–13.

- Nakajima, T., et al. (2014), Formation of pockmarks and submarine canyons associated with dissociation of gas hydrates on the Joetsu Knoll, eastern margin of the Sea of Japan, *J. Asian Earth Sci.*, *90*, 228–242.
- Netzeband, G. L., C. P. Hubscher, D. Gajewski, J. W. G. Grobys, and J. Bialas (2005), Seismic velocities from the Yaquina forearc basin off Peru: Evidence for free gas within the gas hydrate stability zone, *Int. J. Earth Sci.*, *94*(3), 420–432.
- Nickel, J. C., R. di Primio, K. Mangelsdorf, D. Stoddart, and J. Kallmeyer (2012), Characterization of microbial activity in pockmark fields of the SW-Barents Sea, *Mar. Geol.*, *332*, 152–162.
- Noethen, K., and S. Kasten (2011), Reconstructing changes in seep activity by means of pore water and solid phase Sr/Ca and Mg/Ca ratios in pockmark sediments of the Northern Congo Fan, *Mar. Geol.*, *287*(1–4), 1–13.
- Ostanin, I., Z. Anka, R. di Primio, and A. Bernal (2013), Hydrocarbon plumbing systems above the Snøhvit gas field: Structural control and implications for thermogenic methane leakage in the Hammerfest Basin, SW Barents Sea, *Mar. Pet. Geol.*, *43*, 127–146.
- Pape, T., A. Bahr, S. A. Klapp, F. Abegg, and G. Bohrmann (2011), High-intensity gas seepage causes rafting of shallow gas hydrates in the southeastern Black Sea, *Earth Planet. Sci. Lett.*, *307*(1–2), 35–46.
- Prinzhofer, A., and E. Pernaton (1997), Isotopically light methane in natural gas: bacterial imprint or diffusive fractionation?, *Chem. Geol.*, *142*(3), 193–200.
- Reeburgh, W. S. (1976), Methane consumption in Cariaco Trench waters and sediments, *Earth Planet. Sci. Lett.*, *28*(3), 337–344.
- Riboulot, V., A. Cattaneo, S. Berne, R. Schneider, M. Voisset, P. Imbert, and S. Grimaud (2012), Geometry and chronology of late Quaternary depositional sequences in the Eastern Niger Submarine Delta, *Mar. Geol.*, *319*, 1–20.
- Riboulot, V., Y. Thomas, S. Berne, G. Jouet, and A. Cattaneo (2014), Control of Quaternary sea-level changes on gas seeps, *Geophys. Res. Lett.*, *41*, 4970–4977, doi:10.1002/2014GL060460.
- Riboulot, V., N. Sultan, P. Imbert, and S. Ker (2016), Initiation of gas-hydrate pockmark in deep-water Nigeria: Geo-mechanical analysis and modelling, *Earth Planet. Sci. Lett.*, *434*, 252–263.
- Rise, L., J. Sættem, S. Fanavoll, T. Thorsnes, D. Ottesen, and R. Bøe (1999), Sea-bed pockmarks related to fluid migration from Mesozoic bed-rock strata in the Skagerrak offshore Norway, *Mar. Pet. Geol.*, *16*(7), 619–631.
- Ruffine, L., et al. (2013), Investigation on the geochemical dynamics of a hydrate-bearing pockmark in the Niger Delta, *Mar. Pet. Geol.*, *43*, 297–309.
- Ruffine, L., et al. (2015), Pore water geochemistry at two seismogenic areas in the Sea of Marmara, *Geochem. Geophys. Geosyst.*, *16*, 2038–2057, doi:10.1002/2015GC005798.
- Schmidt, M., C. Hensen, T. Morz, C. Muller, I. Grevermeyer, K. Wallmann, S. Mau, and N. Kaul (2005), Methane hydrate accumulation in “Mound 11” mud volcano, Costa Rica forearc, *Mar. Geol.*, *216*(1–2), 83–100.
- Schoell, M. (1983), Genetic characterization of natural gases, *AAPG Bull.*, *67*(12), 2225–2238.
- Seeberg-Elverfeldt, J., M. Schlüter, T. Feseker, and M. Kölling (2005), Rhizon sampling of pore waters near the sediment/water interface of aquatic systems, *Limnol. Oceanogr. Methods*, *3*, 361–371.
- Simonetti, A., J. H. Knapp, K. Sleeper, C. B. Lutken, L. Macelloni, and C. C. Knapp (2013), Spatial distribution of gas hydrates from high-resolution seismic and core data, Woolsey Mound, Northern Gulf of Mexico, *Mar. Pet. Geol.*, *44*, 21–33.
- Sultan, N., M. Voisset, T. Marsset, A. M. Vernant, E. Cauquil, J. L. Colliat, and V. Curinier (2007), Detection of free gas and gas hydrate based on 3D seismic data and cone penetration testing: An example from the Nigerian Continental Slope, *Mar. Geol.*, *240*(1–4), 235–255.
- Sultan, N., et al. (2010), Hydrate dissolution as a potential mechanism for pockmark formation in the Niger delta, *J. Geophys. Res.*, *115*, B08101, doi:10.1029/2010JB007453.
- Sultan, N., et al. (2014), Pockmark formation and evolution in deep water Nigeria: Rapid hydrate growth versus slow hydrate dissolution, *J. Geophys. Res. Solid Earth*, *119*, 2679–2694, doi:10.1002/2013JB010546.
- Sun, R., and Z. Duan (2007), An accurate model to predict the thermodynamic stability of methane hydrate and methane solubility in marine environments, *Chem. Geol.*, *244*(1–2), 248–262.
- Sun, Q., S. Wu, M. Hovland, P. Luo, Y. Lu, and T. Qu (2011), The morphologies and genesis of mega-pockmarks near the Xisha Uplift, South China Sea, *Mar. Pet. Geol.*, *28*(6), 1146–1156.
- Torres, M., K. Wallmann, A. Trehu, G. Bohrmann, W. Borowski, and H. Tomaru (2004), Gas hydrate growth, methane transport, and chloride enrichment at the southern summit of Hydrate Ridge, Cascadia margin off Oregon, *Earth Planet. Sci. Lett.*, *226*(1–2), 225–241.
- Torres, M. E., B. M. A. Teichert, A. M. Trehu, W. Borowski, and H. Tomaru (2004), Relationship of pore water freshening to accretionary processes in the Cascadia margin: Fluid sources and gas hydrate abundance, *Geophys. Res. Lett.*, *31*, L22305, doi:10.1029/2004GL021219.
- Wallmann, K., M. Drews, G. Aloisi, and G. Bohrmann (2006), Methane discharge into the Black Sea and the global ocean via fluid flow through submarine mud volcanoes, *Earth Planet. Sci. Lett.*, *248*(1–2), 545–560.
- Wei, J., et al. (2015), Gas hydrate distributions in sediments of pockmarks from the Nigerian margin – Results and interpretation from shallow drilling, *Marine Pet. Geol.*, *59*, 359–370.
- Whiticar, M. J. (1994), Correlation of natural gases with their sources, in *The Petroleum System: From Sources to Trap*, vol. 60, edited by L. B. Magoon and W. G. Dow, AAPG Mem-American Association of Petroleum Geologists, pp. 261–283.
- Whiticar, M. J. (1999), Carbon and hydrogen isotope systematics of bacterial formation and oxidation of methane, *Chem. Geol.*, *161*(1–3), 291–314.
- Whiticar, M. J., E. Faber, and M. Schoell (1986), Biogenic methane formation in marine and freshwater environments: CO₂ reduction vs. acetate fermentation—Isotope evidence, *Geochim. Cosmochim. Acta*, *50*(5), 693–709.
- Yoshinaga, M. Y., T. Holler, T. Goldhammer, G. Wegener, J. W. Pohlman, B. Brunner, M. M. M. Kuypers, K.-U. Hinrichs, and M. Elvert (2014), Carbon isotope equilibration during sulphate-limited anaerobic oxidation of methane, *Nat. Geosci.*, *7*(3), 190–194.